HERON is jointly edited by:
STEVIN-LABORATORY of the department of Civil Engineering, Delft University of Technology, Delft, The Netherlands
and
INSTITUTE TNO for Building Materials and Building Structures. Rijswijk (ZH), The Netherlands.
HERON contains contributions based mainly on research work performed in these laboratories on strength of materials, structures and materials science.

ISSN 0046-7316

HERON vol. 30 1985 no. 1

Contents

SMEARED CRACK APPROACH AND FRACTURE LOCALIZATION IN CONCRETE

J. G. Rots[2], *P. Nauta*[1], *G. M. A. Kusters*[1], *J. Blaauwendraad*[2]

[1] Institute TNO for Building Materials and Building Structures
Software Engineering Department - DIANA Section
P.O. Box 49, 2600 AA Delft, The Netherlands

[2] Delft University of Technology
Department of Civil Engineering - Structural Mechanics Group
P.O. Box 5048, 2600 GA Delft, The Netherlands

This publication has been issued in close co-operation with the Netherlands Committee for Research, Codes and Specifications for Concrete (CUR-VB) and the Netherlands Technology Foundation (STW).

Publications in HERON since 1970

SMEARED CRACK APPROACH AND FRACTURE LOCALIZATION IN CONCRETE

Summary

The possibilities of the smeared crack concept for simulating crack propagation and fracture in concrete is investigated. A smeared crack formulation is proposed which treats concrete constitutive behaviour separately from crack interface behaviour. In this study concrete is in most cases modelled as having linearly elastic characteristics. For the crack (or the band of micro-cracks) tensile strain-softening and shear transfer are allowed to take place but no interaction between these phenomena is taken into account. A crack closing option is included.

The model has been evaluated by using the DIANA finite element package. Three types of example problems are considered.

First, mode I fracture in unreinforced concrete is discussed. Emphasis is placed upon the effect of the basic concrete softening properties, such as the shape of the strain-softening branch and the value of the fracture energy G_f. The way in which stable and mesh-insensitive solutions can be obtained is demonstrated.

Next, mixed-mode fracture in unreinforced concrete is discussed. Here, the predicted post-peak response is shown to be unstable, which has to do with the existence of a considerable number of cracks of which only a limited number is active while the majority is arrested or closed. Again mesh-sensitivity of the results is examined, not only with respect to mesh refinements but also with respect to a change in the orientation of mesh lines. Very fine meshes seem to be most promising for reproducing curvilinear crack trajectories.

Finally, mixed-mode fracture in two shear-critical reinforced beams is analysed, one of which fails in diagonal tension and one in shear-compression. Sudden extensive diagonal cracking is shown to be simulated quite correctly, although it should be added that corresponding genuine limit loads are not always attained. Further, comments are made on the crack shear representation adopted, involving a constant shear retention factor.

The principal outcome of the project is that pronounced fracture localization can in principle be predicted by using a smeared crack strategy. However, problems are also encountered to which no definite answers can yet be given. Throughout the article possible future approaches are indicated which may help to solve them.

Smeared crack approach and fracture localization in concrete

1 Introduction

1.1 *General*

The nonlinear response of concrete is frequently dominated by progressive cracking resulting in localized failure. In this context we may, for instance, think of diagonal tension cracks that suddenly occur and dominate the failure behaviour of shear-critical reinforced beams.

It is this local deformation within discrete cracks that inspired some researchers to develop so-called discrete crack models (e.g. Ngo & Scordelis, 1967, Blaauwendraad & Grootenboer, 1981, Hillerborg, 1984, Ingraffea & Saouma, 1984). With such an approach the geometrical discontinuities due to cracking are incorporated within the idealization of the structure.

Another, more commonly adopted procedure for dealing with cracks is the "smeared crack" concept (e.g. Rashid, 1968, Suidan & Schnobrich, 1973, Bažant et al., 1979–1983). With this continuum approach the local discontinuities are distributed over some tributary area within the finite element. Hence, relative displacements of crack surfaces are represented by crack strains and the constitutive behaviour of cracked concrete can be modelled in terms of stress-strain relations. Contrary to the discrete crack concept, the smeared crack concept fits the nature of the finite element displacement method, as the continuity of the displacement field remains intact.

The smeared crack strategy, however, has not escaped criticism. The prime objection voiced against it was that it would tend to spread crack formation over the entire structure so that it would be incapable of predicting local fracture.

One of the main objectives of the present study is to demonstrate that the latter statement is not necessarily true. It will be explained that the smeared crack concept can lead to realistic predictions of local concrete fracture provided that the crack model properly takes into account the effects of tensile strain-softening due to progressive micro-cracking and of crack closing. A number of examples for both plain (unreinforced) and reinforced concrete will be presented. The examples include mode I (only crack opening displacements) as well as mixed-mode fracture problems (crack opening as well as crack sliding displacements). In order to examine the latter type of problems, the smeared crack model has been formulated in such a way that not only tensile strain-softening but also crack shear can be taken into account.

The work is based on two 1983 reports and on a recent paper, which are included in the reference list as Rots (1983a, 1983b) and Rots, Kusters & Blaauwendraad (1984). It is not intended to provide definite solutions but rather to trace current difficulties encountered in concrete mechanics and to indicate some approaches to be adopted in future investigations.

The numerical results reported here have been obtained with the DIANA finite element package which offers a wide range of options for nonlinear analyses. For a general overview of this package the reader is referred to papers by De Borst, Nauta, Kusters & De Witte (1983, 1984).

1.2 *Concrete tensile strain-softening behaviour*

Crack propagation and fracture are primarily bound up with the behaviour of the material in tension. Let us therefore start with a brief summary of what is known about concrete response in tension.

Several experiments have revealed that this response is primarily controlled by the formation of micro-cracks (e.g. Evans & Marathe, 1968, Heilmann, Hilsdorf & Finsterwalder, 1969, Petersson, 1981 and Reinhardt, 1984). Initially a limited number of such cracks develop anywhere in the specimen, but if somewhere in the specimen the tensile stress reaches a certain strength limit f_i all additional deformation due to micro-cracks will localize within a so-called fracture zone. Fig. 1.1a shows an example of a fracture zone originated at the tip of a (macro-)crack or notch.

Within a fracture zone the stress gradually decreases while the strain increases, as shown in Fig. 1.1b. This phenomenon is known as tensile strain-softening. When the end of the descending branch is approached, the micro-cracks coalesce into one continuous macro-crack.

Strain localization within a fracture zone is accompanied by unloading of the material outside the fracture zone, which means that the micro-cracks outside the fracture zone are arrested or even closed. Typical unloading curves for closing micro-cracks are shown in Fig. 1.1c.

For a more detailed description of concrete tension-softening behaviour the reader is referred to, for example, Hillerborg (1984).

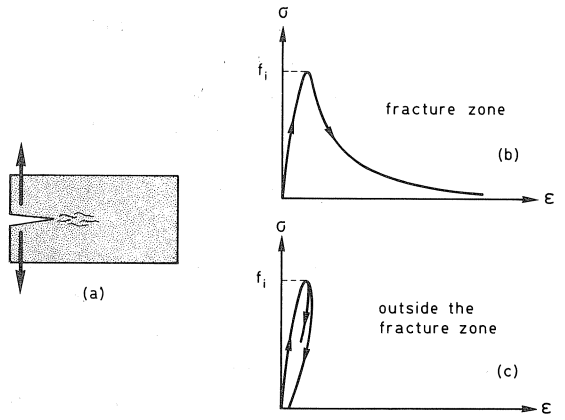

Fig. 1.1. (a) a fracture zone of micro-cracks
(b) tensile strain-softening within a fracture zone
(c) unloading outside a fracture zone.

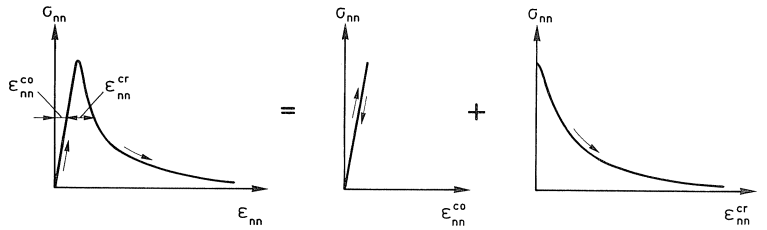

Fig. 1.2. Resolution of the total strain ε_{nn} of a fracture zone into concrete strain ε_{nn}^{co} and crack strain ε_{nn}^{cr}.

In adopting a smeared crack approach it is of crucial importance to interpret the strain within a fracture zone. As illustrated in Fig. 1.2, this strain may be resolved into two distinct parts:

- The strain ε_{nn}^{co} of the concrete in between the micro-cracks.
  This part of the strain is considered to be merely elastic because experiments indicate that nonlinearity of the ascending branch of the tensile stress-strain curve can be neglected, as shown in the diagram.
- The crack strain ε_{nn}^{cr} representing the opening of micro-cracks.
  This part of the strain only acts over a limited width, namely the width of the fracture zone or, in the case of finite element modelling, the width of the finite element over which the micro-cracks are smeared out. As a consequence of this the crack strain should always be envisaged in close relation to this width, and this introduces a size effect into the strain-softening formulation. In fact, the strain-softening modulus has to be adjusted to the chosen size of the finite elements, for otherwise the fracture energy release would be mesh-dependent.
  This approach was pioneered by Bažant & Oh (1983) and in now becoming customary, as may be concluded from the work of for instance Nilsson & Oldenburg (1982), Glemberg (1983), Willam (1984), Bićanić, Sture, Hurlbut & Day (1984), Crisfield (1984) and Leibengood, Darwin & Dodds (1984).

In the present study both the resolution of the strain field and the size effect in the strain-softening formulation are dealt with, as will be explained in Chapters 2 and 3 respectively. These two features make possible an adequate description of concrete tensile strain-softening within the context of the smeared crack strategy.

2 Smeared crack model including the effect of tensile strain-softening

2.1 *Essentials*

The basic assumption of the proposed model is the resolution of the field of total strain increments into concrete strain increments and crack strain increments:

$$\Delta\boldsymbol{\varepsilon} = \Delta\boldsymbol{\varepsilon}^{co} + \Delta\boldsymbol{\varepsilon}^{cr} \tag{2.1}$$

in which

$\Delta\boldsymbol{\varepsilon}$ = vector of total global strain increments
$\Delta\boldsymbol{\varepsilon}^{co}$ = vector of concrete global strain increments
$\Delta\boldsymbol{\varepsilon}^{cr}$ = vector of crack global strain increments

The prime advantage of this resolution is that it allows the crack interface behaviour to be treated separately from the constitutive behaviour of the concrete between the cracks. This approach has also been adopted by Litton (1976) and Bažant & Gambarova (1980). It differs from some traditional smeared crack models that take their starting point in a mixed stress-strain relation for cracked concrete (e.g. Rashid, 1968, Suidan & Schnobrich, 1973, Hand, Pecknold & Schnobrich, 1973, Lin & Scordelis, 1975).

A consequence of the resolution is that it allows for a further sub-resolution of the concrete strain field and the crack strain field themselves. The concrete strain may for instance be composed of elastic, plastic, creep and thermal strains. This enables cracking to be combined with other nonlinear material effects. Similarly, the crack strain field may be composed of the separate contributions of a number of individual cracks that simultaneously occur at one sampling point. Such a sub-decomposition of the crack strain field has been applied by Litton (1976) and, in a more general way, by De Borst & Nauta (1984).

2.2 *Crack strains and crack interface stresses*

Let us consider the crack morphology shown in Fig. 2.1. For the case of plane stress we have two relative displacements between the crack faces, namely a crack opening displacement COD and a crack sliding displacement CSD. The subscripts n and t refer to the directions normal to the crack and tangential to the crack respectively.

With the smeared approach the crack opening displacement is replaced by a normal local crack strain ε_{nn}^{cr} and the crack sliding displacement is replaced by a shear local crack strain γ_{nt}^{cr}. The global crack strains are obtained by transforming the local crack strains to the global coordinate system:

$$\begin{bmatrix} \varepsilon_{xx}^{cr} \\ \varepsilon_{yy}^{cr} \\ \gamma_{xy}^{cr} \end{bmatrix} = \begin{bmatrix} \cos^2\theta & -\sin\theta\cos\theta \\ \sin^2\theta & \sin\theta\cos\theta \\ 2\sin\theta\cos\theta & \cos^2\theta - \sin^2\theta \end{bmatrix} \begin{bmatrix} \varepsilon_{nn}^{cr} \\ \gamma_{nt}^{cr} \end{bmatrix}$$

or

$$\boldsymbol{\varepsilon}^{cr} = \mathbf{N}\mathbf{e}^{cr} \tag{2.2}$$

in which

$\boldsymbol{\varepsilon}^{cr}$ = vector of global crack strains
$\mathbf{e}^{cr}$ = vector of local crack strains, i.e. the crack strains with respect to the crack axes
θ = the angle from the global x-axis to the normal of the crack
$\mathbf{N}$ = crack strain transformation matrix

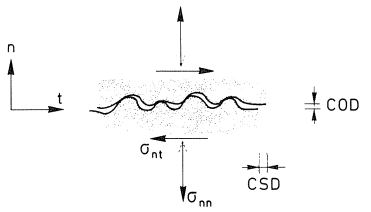

Fig. 2.1. Crack interface stresses and relative displacements.

Fig. 2.1 also shows the crack interface stresses. For the case of plane stress we have a normal interface stress σ_{nn}^{cr} and a shear interface stress σ_{nt}^{cr}. The crack interface stress vector is related to the global stress vector:

$$\begin{bmatrix} \sigma_{nn}^{cr} \\ \sigma_{nt}^{cr} \end{bmatrix} = \begin{bmatrix} \cos^2\theta & \sin^2\theta & 2\sin\theta\cos\theta \\ -\sin\theta\cos\theta & \sin\theta\cos\theta & \cos^2\theta - \sin^2\theta \end{bmatrix} \begin{bmatrix} \sigma_{xx} \\ \sigma_{yy} \\ \sigma_{xy} \end{bmatrix}$$

or

$$\mathbf{s}^{cr} = \mathbf{N}^T\boldsymbol{\sigma} \tag{2.3}$$

in which

$\mathbf{s}^{cr}$ = vector of crack interface stresses
$\boldsymbol{\sigma}$ = global stress vector
$\mathbf{N}^T$ = the crack stress transformation matrix, which is the transpose of the crack strain transformation matrix

If multiple cracks occur at one sampling point, the global crack strain vector may be composed of the individual local crack strain vectors $\mathbf{e}_i^{cr}$:

$$\boldsymbol{\varepsilon}^{cr} = \sum_i \mathbf{N}_i\mathbf{e}_i^{cr} \tag{2.4}$$

where $\mathbf{N}_i$ is the strain transformation matrix for crack number *i*. Further, each individual crack stress vector $\mathbf{s}_i^{cr}$ may be related to the global stress vector:

$$\mathbf{s}_i^{cr} = \mathbf{N}_i^T\boldsymbol{\sigma} \tag{2.5}$$

In the following the model is elaborated for the case that only one crack occurs at a sampling point. The elaboration for multiple cracking is given by De Borst & Nauta (1984), who properly assemble individual crack strains, individual crack stresses and individual transformation matrices. Further, attention is confined to plane stress conditions. Extension to axi-symmetrical and three-dimensional stress states is possible. In the latter case two crack shear displacements and two shear interface stresses have to be considered instead of only one.

2.3 *Crack interface relation*

The crack interface stresses are assumed to be incrementally related to the local crack strains:

$$\Delta \mathbf{s}^{cr} = \mathbf{D}^{cr} \Delta \mathbf{e}^{cr} \tag{2.6}$$

The crack interface matrix $\mathbf{D}^{cr}$ may reflect effects like tensile strain-softening, aggregate interlock and crack dilatancy. In the present study $\mathbf{D}^{cr}$ is filled as follows:

$$\mathbf{D}^{cr} = \begin{bmatrix} D_c & 0 \\ 0 & G_c \end{bmatrix} \tag{2.7}$$

in which

- $D_c = D_c^o < 0$ for active cracks, i.e. cracks that are opening
  $D_c = D_c^c > 0$ for arrested cracks, i.e. cracks that start closing
  D_c^o is the tensile strain-softening modulus and for D_c^c the secant stiffness is used, as indicated in Fig. 2.2a.
  One a crack has fully closed again, which means that its unloading path in Fig. 2.2a has passed the origin, the material is assumed to behave in the same way as if it were uncracked. Further, cracks are allowed to re-open, re-close and so on.
  In this study updates of the structural stiffness matrix, which are required if a Newton-type solution procedure is adopted, are always based on the use of the positive secant stiffness D_c^c, not only for arrested cracks but also for active ones. To generate the out-of-balance force vector the negative softening modulus D_c^o is used for active cracks and the positive secant stiffness D_c^c is used for arrested cracks.
- G_c is the crack shear modulus as indicated in Fig. 2.2b.

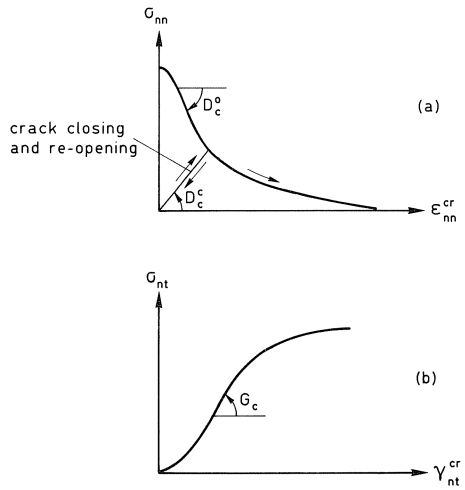

Fig. 2.2. Definition of crack interface stiffnesses D_c^o, D_c^c, and G_c.

In principle, the model permits D_c and G_c to be chosen arbitrarily. Hence, the analyst can specify any nonlinear shape of the curves in Fig. 2.2 he desires. For the present study we confined ourselves to the use of simple linear or multilinear diagrams, as will be outlined in Chapter 3.

The assumption of zero off-diagonal terms in equation (2.7) implies no interaction between normal stress transfer and shear stress transfer across cracks. When local softening behaviour at a crack tip is of prime interest this assumption is not expected to have serious consequences. This is because cracks in concrete mostly propagate in such a way that mode I prevails at the crack tip so that neither the off-diagonal terms nor G_c will have significant influence. On the other hand, when attention is directed towards global behaviour of macro-cracks, interaction is certainly present. Then, the aggregate particles protruding from the surfaces of the macro-crack cause crack shear displacements to accompany crack opening displacements (crack dilatancy, see for instance Walraven, 1980, Bažant & Gambarova, 1980). Although the model offers the possibility to account for crack dilatancy, this has not been done in the present study.

2.4 *Concrete stress-strain relation*

Just as for the crack, a constitutive relation may be defined for the concrete:

$$\Delta\boldsymbol{\sigma} = \mathbf{D}^{co}\Delta\boldsymbol{\varepsilon}^{co} \tag{2.8}$$

This relation may represent effects like elasticity, plasticity, creep and so on. In the present study attention is primarily directed towards crack behaviour; therefore the concrete is simply assumed to behave in a linearly elastic manner, unless specifically stated otherwise. Hence, $\mathbf{D}^{co}$ is the well-known matrix according to Hooke's law which is defined by Young's modulus E and Poisson's ratio ν.

For most of the example problems considered it was checked that the maximum compressive stress remained small compared with the compressive strength, so that the assumption of elasticity under compression does not detract much from the usefulness of the computations.

2.5 *Stress-strain relation for cracked concrete*

By suitably combining the equations given in the preceding section the stress-strain relation for cracked concrete can be formulated. The starting point is taken in a combination of equations (2.1), (2.2) and (2.8):

$$\Delta\boldsymbol{\sigma} = \mathbf{D}^{co}[\Delta\boldsymbol{\varepsilon} - \mathbf{N}\Delta\mathbf{e}^{cr}] \tag{2.9}$$

The second step is to relate increments of local crack strain to increments of total strain. This may be accomplished by combining equations (2.3) and (2.6) to

$$\mathbf{D}^{cr}\Delta\mathbf{e}^{cr} = \mathbf{N}^{T}\Delta\boldsymbol{\sigma} \tag{2.10}$$

and substituting this into equation (2.9), which yields

$$\Delta \mathbf{e}^{cr} = [\mathbf{D}^{cr} + \mathbf{N}^T \mathbf{D}^{co} \mathbf{N}]^{-1} \mathbf{N}^T \mathbf{D}^{co} \Delta \boldsymbol{\varepsilon} \tag{2.11}$$

Finally, the relation between increments of total stress and increments of total strain is obtained by substituting equation (2.11) back into equation (2.9):

$$\Delta \boldsymbol{\sigma} = [\mathbf{D}^{co} - \mathbf{D}^{co} \mathbf{N} [\mathbf{D}^{cr} + \mathbf{N}^T \mathbf{D}^{co} \mathbf{N}]^{-1} \mathbf{N}^T \mathbf{D}^{co}] \Delta \boldsymbol{\varepsilon} \tag{2.12}$$

In this way cracking is dealt with in a manner similar to plasticity. The effect is that the elastic stiffness $\mathbf{D}^{co}$ is reduced.

2.6 *Alternative formulation of the model*

As mentioned before, the advantage of the present model is that it allows crack interface behaviour to be treated separately from concrete behaviour. However, it can be shown that under certain conditions the present model becomes equivalent to a directly formulated stress-strain relation for cracked concrete, namely the mode I crack band model proposed by Bǎzant & Oh (1983), which can be extended to a mixed-mode model, e.g. Rots (1983a, 1983b). The conditions are:

- only one crack occurs at a sampling point;
- the off-diagonal terms in equation (2.7) are zero;
- concrete behaves in a linearly elastic manner.

The comparison between the two models is worked out in detail in Appendix I.

For most of the example problems considered in this study the above mentioned conditions are satisfied. Hence the results could quite as well have been obtained by using the directly formulated model. The advantage of the present formulation becomes especially manifest if one or more of the above mentioned conditions are violated.

3 Crack parameters

3.1 *Tensile strain-softening parameters*

The strain-softening diagram shown in Fig. 3.1a is defined by

a. the strength limit f_i for which a fracture zone is initiated;
b. the area g_f under the diagram;
c. the shape of the descending branch.

Re a. Strength limit f_i.

In the present study the strength limit f_i is assumed to be constant and equal to the uniaxial tensile strength f_{ct}. The model, however, permits f_i to be made a function of for instance the compressive stress in the lateral direction. This anables the "tension cut-off" to be more closely adjusted to biaxial or triaxial test data.

Re b. Area g_f under the diagram.

The area g_f under the curve can be expressed as

$$g_f = \int \sigma_{nn} \, d\varepsilon_{nn}^{cr} \tag{3.1}$$

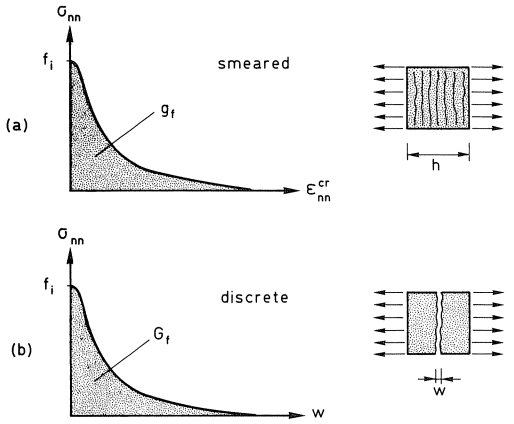

Fig. 3.1. (a) Tensile stress vs. crack strain diagram
(b) Tensile stress vs. crack opening displacement diagram
The diagrams are defined by the strength limit f_i, the area under the diagram and by the shape of the diagram.

It can be linked with the fracture energy G_f, which is assumed to be a material property. G_f is defined as the amount of energy required to create one unit of area of a continuous crack, and can be expressed as (Hillerborg, 1984):

$$G_f = \int \sigma_{nn}\, dw \tag{3.2}$$

in which w represents the sum of the opening displacements of all micro-cracks within the fracture zone, schematically shown in Fig. 3.1b.

With the smeared approach w is represented by a crack strain acting over a certain width within the finite element, which will be called the crack band width h, as indicated in Fig. 3.1a. As w is the accumulated crack strain, we have

$$w = \int_h \varepsilon_{nn}^{cr}\, dn \tag{3.3}$$

Assuming the micro-cracks to be uniformly distributed over the crack band, eq. (3.3) simply becomes

$$w = h\varepsilon_{nn}^{cr} \tag{3.4}$$

Combination of (3.4) with (3.1) and (3.2) yield the relation between g_f and G_f

$$G_f = hg_f \tag{3.5}$$

In Appendix II it is explained that the actual magnitude of h depends on the chosen element size, element type, element shape, integration scheme, and on the particular problem considered (symmetric or not, curvilinear or straight crack path, etc.). Appendix II also indicates the cases for which the assumption of uniform strain over the crack band is justified.

Re c. Shape of the descending branch.
In the present study either a linear or a bilinear descending branch, as proposed by Petersson (1981) and Hillerborg (1984), has been applied, as shown in Fig. 3.2. On working out equation (3.5) for these two cases, it appears that the strain-softening modulus D_c^o has to be adjusted to the chosen crack band width:

linear softening:

$$D_c^o = -\tfrac{1}{2}\frac{f_{ct}^2 h}{G_f} \tag{3.6}$$

bilinear softening:

$$\begin{aligned} D_c^o &= -\tfrac{5}{6}\frac{f_{ct}^2 h}{G_f} \quad \text{if} \quad 0 < \varepsilon_{nn}^{cr} < \tfrac{2}{9}\varepsilon_u \\ D_c^0 &= -\tfrac{5}{42}\frac{f_{ct}^2 h}{G_f} \quad \text{if} \quad \tfrac{2}{9}\varepsilon_u < \varepsilon_{nn}^{cr} < \varepsilon_u \end{aligned} \tag{3.7}$$

The adjustment of D_c^o to h is bound up with the fact that the ultimate strain ε_u of the descending branch is adjusted to h in a similar way, as shown in Fig. 3.2.

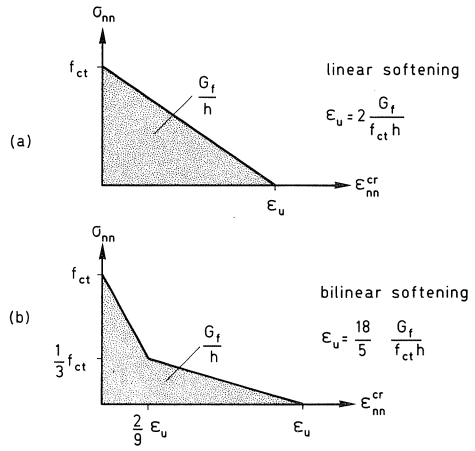

Fig. 3.2. In the present study either a linear or a bilinear softening diagram is employed.

3.2 *Crack shear modulus*

Unless otherwise stated, the crack shear modulus G_c is assumed to be a constant, as shown in Fig. 3.3.

3.3 *Alternative representation of crack parameters*

Within smeared crack models that are not based upon resolution of strains (e.g. Suidan & Schnobrich, 1973, Hand, Pecknold & Schnobrich, 1973, Lin & Scordelis, 1975, and

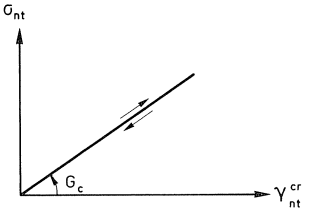

Fig. 3.3. In the present study the crack shear modulus G_c is assumed to be a constant.

the model mentioned in Section 2.6 and Appendix I) it has become accepted practice to represent the shear stiffness of cracked concrete by means of a shear retention factor β, indicating the percentage of elastic shear capacity that is retained after cracking. As a consequence the initial shear capacity G is reduced to βG once the material has cracked. Further, some of such directly formulated models are based upon the use of a softening modulus E_t. The parameters βG and E_t are associated with the total strain, whereas the parameters G_c and D_c^o of the present model are associated solely with the crack strain.

It is instructive to verify the agreement between the parameters for the two types of models. The fact that the off-diagonal terms in the crack interface matrix (2.7) are assumed to be zero allows us to do so. This assumption implies that the concrete normal stiffness E and the crack normal stiffness D_c^o act like springs connected in series. In this way we obtain for the tensile stiffness

$$\frac{1}{E}+\frac{1}{D_c^o}=\frac{1}{E_t} \tag{3.8}$$

so that D_c^o can be expressed in terms of E and E_t:

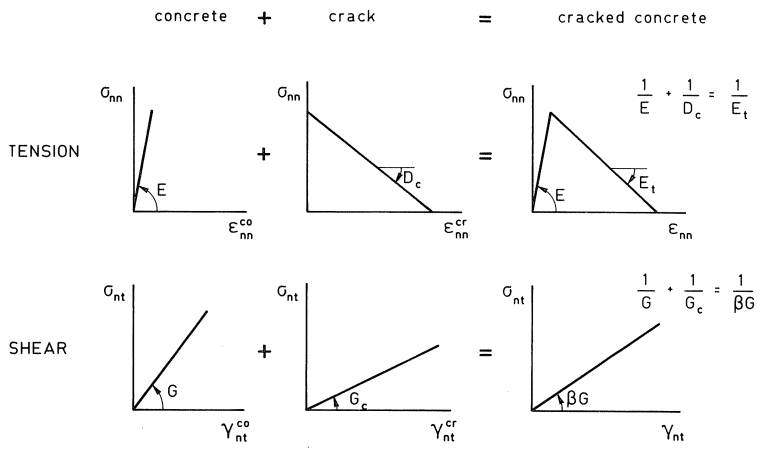

Fig. 3.4. Illustration of series arrangement of concrete and crack.

$$D_c^o = \frac{EE_t}{E - E_t} \tag{3.9}$$

Along similar lines one obtains for the shear stiffness

$$\frac{1}{G} + \frac{1}{G_c} = \frac{1}{\beta G} \tag{3.10}$$

so that G_c can be expressed in terms of β and G

$$G_c = \frac{\beta}{1 - \beta} G \tag{3.11}$$

The series arrangement is illustrated in Fig. 3.4.

4 Mode I fracture in unreinforced concrete

4.1 *Notched beam*

From among the great variety of mode I fracture experiments a notched beam of unreinforced concrete, tested by Petersson (1981), was selected for analysis. Two major advantages of this beam experiment are that it has been repeated several times and that the necessary material parameters, such as G_f, have been carefully specified. This allows the numerical results to be fairly matched with the experimental results.

Finite element meshes, dimensions and material parameters are shown in Fig. 4.1. In this section only computations on the fine mesh will be considered; comparisons with the coarse mesh are given in the next section. The meshes consist of quadratic isoparametric elements, numerically integrated by means of the nine-point Gaussian scheme. In the mesh transition region the free nodes were properly tied to the others in order to achieve compatibility. Note that the notch was modelled as an element-wide gap.

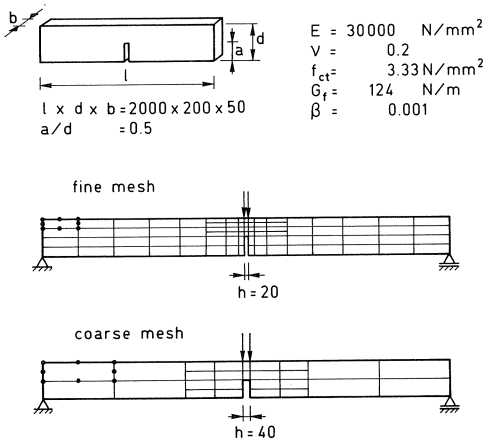

Fig. 4.1. Data and finite element meshes for notched unreinforced beam in mode I fracture (dimensions in mm).

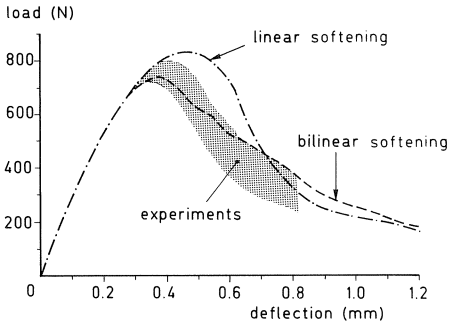

Fig. 4.2. Load-deflection response for notched beam in mode I fracture (computations on fine mesh).

The experiments as well as the analyses were performed by incrementing the displacement at the center of the beam. The numerical solution was computed by using the Modified Newton-Raphson iteration scheme, as has been done for all the example problems reported in this study.

Fig. 4.2 compares experimental and numerical load-deflection curves. For the same value of G_f two different shapes of the softening diagram have been used, namely the linear and the bilinear, according to Fig. 3.2. An accurate fit of the experiment is obtained when the bilinear softening diagram is applied. In contrast, the linear softening diagram leads to a solution that clearly lies outside the experimental scatter. Generally speaking, the numerical solution for such type of fracture problems is found to be extremely sensitive to the input of the basic softening properties, i.e. the shape of the softening branch and the value of G_f.

It is surprising that not only the maximum load but also the post-peak response of the beam can be satisfactorily simulated. This was achieved by adopting a very low shear retention factor of 0.001. For high values of β the calculated residual post-peak strength is not correct. At first sight this influence of β may look peculiar, because for mode I experiments no crack shear is to be expected. However, when plotting the cracks at the Gauss-points, as has been done in Fig. 4.3, it can be observed that only the

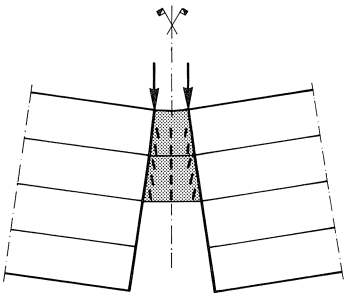

Fig. 4.3. Typical crack pattern for a mode I problem. Off-centre Gauss-points have non-vertical cracks.

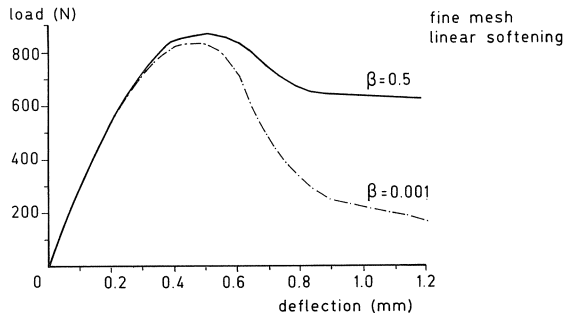

Fig. 4.4. Effect of shear retention factor β on load-deflection response for notched beam in mode I fracture. A low value is required to achieve correct post-peak response.

Gauss-points at the centre of the crack band contain purely vertical mode I cracks, whereas the off-centre points contain inclined cracks along which shear strains are being produced. In order to avoid energy consumption in crack shear a very low value of β should be adopted. Otherwise, the residual post-peak strength of the beam is considerably overestimated, as shown in Fig. 4.4. In future the authors will apply single-point integration techniques, which is a more elegant way to avoid problems.

It should be noted that all Gauss-points in the crack band contain active cracks. Crack arresting or crack closing does not occur, but unloading only takes place elastically, outside the crack band. Here, the crack band is predicted to be of single element width, but if very fine meshes are used, as for instance has been done by Leibengood, Darwin & Dodds (1984), the crack band width may amount to several times the element width. In that case some of the off-centre cracks are found to be arrested or closed. Some further comments on the use of very fine meshes will be made in the next Section.

Further details about the analysis, such as stress-profiles at mid-section, are given by Rots (1983a).

Finally it is mentioned that Petersson (1981) analysed the beam not only experimentally but also numerically by using a discrete type of crack model. It is interesting to note that his numerical results are very similar to those presented here, indicating that it does not matter whether a mode I fracture zone is treated as a blunt crack band or as a sharp discrete crack.

4.2 *Objectivity with respect to element sizes*

An objection often raised against models that are solely based upon strength but not upon energy ("strength-criteria") is that they produce inobjective results that strongly depend upon the analyst's choice of the element sizes (Bažant & Cedolin, 1979, 1983). Using the beam example of the preceding section, it will be verified that this is not the case if softening is applied. For this purpose the notched beam has once again been analysed by using twice as coarse a mesh, as already shown in Fig. 4.1. Attention is confined to a linear softening branch, but for a different shape of the softening branch mesh-objectivity can be demonstrated in a similar way.

Fig. 4.5 shows that the calculated load-deflection curves are essentially the same for the coarse and the fine mesh. The adjustment of the softening modulus D_c^o to the crack band width h according to equation (3.6) obviously assures that the correct value of the fracture energy is consumed in the formation of the mode I crack in front of the notch. This objectivity, explored by Bažant & Oh (1983), means that the structural analyst is free in chosing his element sizes, which is of utmost importance for practical usefulness of such computations.

However, there are some limitations. Firstly, there is a certain upper limit for h, which has been pointed out by Bažant & Oh (1983). In the analysis of large stuctures like dams this limit may be exceeded and in that case the introduction of a mesh-dependent strength limit becomes attractive (Bažant et al., 1979, 1983). Secondly, Bažant (1984) and Bažant, Belytschko & Chang (1984) have stated that there exists also a lower limit for the value that may be used for h, which roughly equals about three times the aggregate size. They pointed out that this lower limit has to do with the fact that the present formulation of the crack band model is based on the local continuum theory. This theory would be unable to produce a detailed resolution of the stress and strain fields within and near the strain-softening region. To overcome these limitations, they proposed a nonlocal continuum theory, which allows arbitrarily fine meshes to be employed.

For the sake of completeness the "no-softening" solutions have been included in Fig. 4.5 (strength-criterion). They are peculiar and inobjective. The finer the mesh, the lower is the predicted maximum load. Clearly, the introduction of the energy parameter G_f turns out to be necessary.

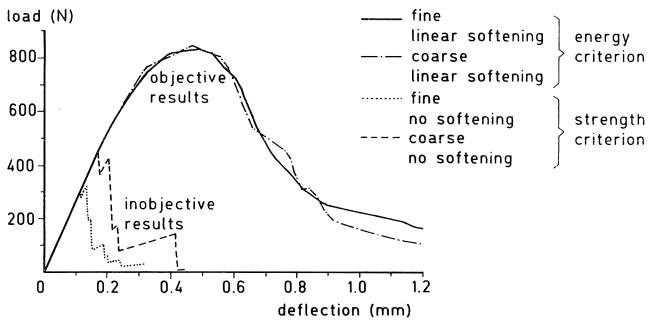

Fig. 4.5. A strength criterion (without softening) yields inobjective results with respect to mesh refinements. An energy criterion (with softening) is essential to achieve objectivity.

4.3 *Double-cantilever beam*

For notched beams the distance between the tip of the notch and the top of the specimen is rather small. As a result of this the compression zone at the top of the beam may obstruct full development of the fracture zone. A specimen which prevents such obstruction is the double-cantilever beam (DCB).

Fig. 4.6a shows a DCB tested by Sok, Baron & François (1979). As the specimen was very large compared with the usual dimensions handled in laboratories, they had to

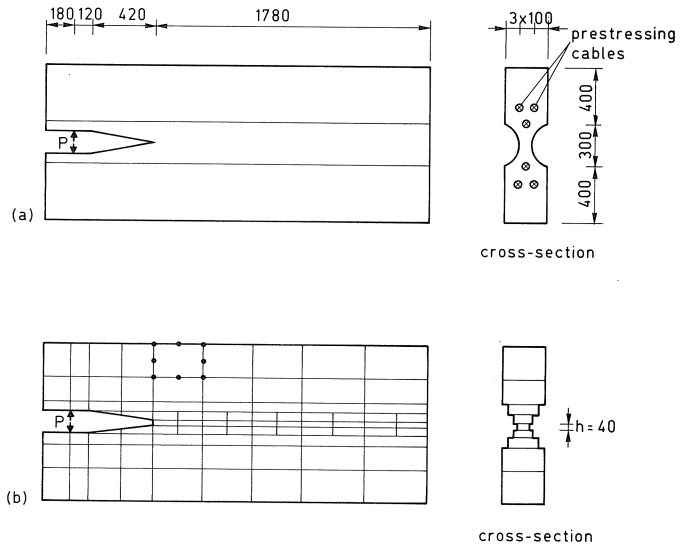

Fig. 4.6. Experimental set-up (a) and finite element mesh (b) for double-cantilever beam in mode I fracture (dimensions in mm).

take some special precautions. First, the specimen thickness at mid-section was reduced so that the crack was forced to follow a straight path. Further, a prestress was applied parallel to the expected crack path.

The finite element idealization is shown in Fig. 4.6b. As indicated, the reduction of specimen thickness was taken into account. In the first instance the prestress had been ignored. This, however, introduced problems, as a number of Gauss-points were predicted to crack not only in the direction parallel to the expected crack path but also in the direction perpendicular to this path. This secondary cracking was attributable to the existence of high bending stresses in the cantilevers. It possibly explains why Sok et al. added a prestress. In the final computations the prestress was taken into account by means of applied loads introducing a uniaxial compression field of 3 N/mm^2.

In Fig. 4.7 the load is plotted against the Crack Mouth Opening Displacement (CMOD). The computations were performed for linear softening as well as bilinear softening. In both cases the G_f value was so determined that the maximum load level corresponds to the value found experimentally. For this beam bilinear softening appears to be superior to linear softening, as it closely resembles the tough behaviour of the beam, indicated by the horizontal plateau at maximum load, whereas linear softening does not.

The development of the fracture zone is represented in Fig. 4.8, which shows stress profiles in front of the notch together with plots of the deformations, corresponding to three different CMOD-levels. Initially the fracture zone is only partially developed, but when it is fully developed it preserves its maximum length for quite a long time till fracture is completed, indicated by a sudden decrease of the load. The diagram also shows the macro-crack advancing behind the fracture zone.

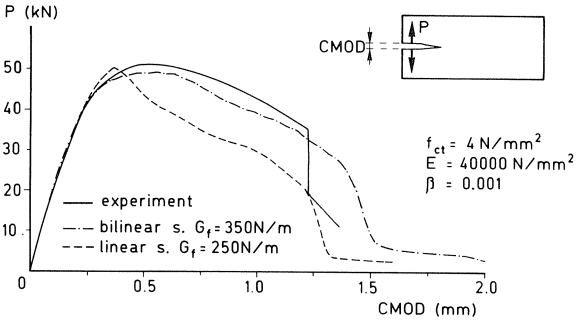

Fig. 4.7. Load-CMOD response for double-cantilever beam (CMOD = Crack Mouth Opening Displacement).

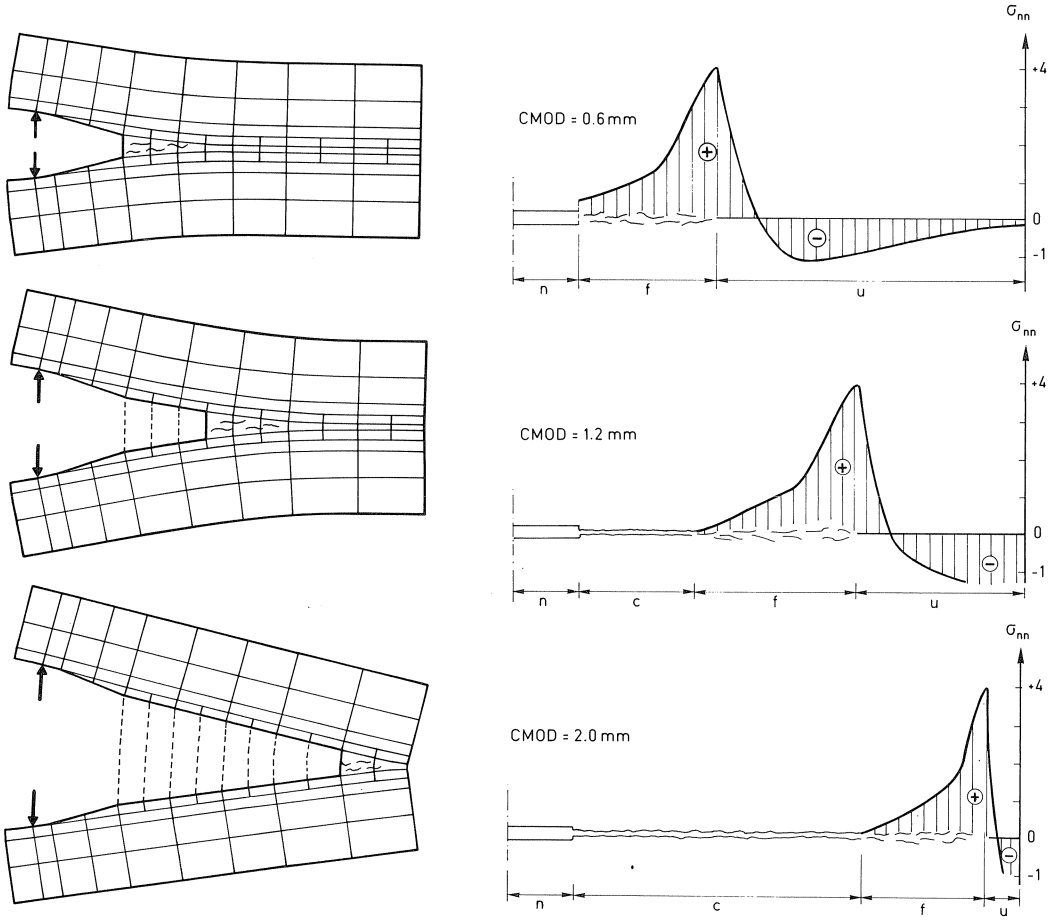

Fig. 4.8. Finite element results for double-cantilever beam (bilinear softening). Deformed meshes (amplification factor 450) and stress-distributions in front of the notch. The position of the notch (n), the macro-crack (c), the fracture zone with micro-cracks (f) and the uncracked part (u) are indicated
(a) CMOD = 0.6 mm, (b) CMOD = 1.2 mm, (c) CMOD = 2.0 mm.

In Fig. 4.8 the distinction between micro-cracks and macro-cracks has been based upon the ultimate strain ε_u of the softening branch (see Fig. 3.2). Such a distinction, however, is quite arbitrary, as the softening branch in reality shows a very long "tail" which makes it difficult to judge when the micro-cracks really coalesce into a macro-crack. As a consequence, a numerical prediction of the length of a fracture zone can not fairly be compared with experimental measurements. (For the DCB Sok et al. (1979) report the fracture zone to have a length of about 200 mm, bilinear softening predicts about 500 mm and linear softening, with the smaller ε_u, predicts 250 mm). On the other hand, comparisons between numerical results obtained with identical softening branches are not confusing. Within this context, it can be stated that the fracture zone predicted for the DCB is four times as long as was predicted for the notched beam of Petersson (Rots, 1983a).

4.4 *Doubt as to the size-independence of the facture energy*

Despite the overwhelming number of fracture experiments there is still lack of knowledge about the basic tensile strain-softening parameter G_f for a certain type of concrete quality. Therefore, an attempt was made to ascertain the G_f-values that bring about the optimum fits of experimental maximum load data, both for linear softening and for bi-linear softening. In addition to the experiments described in the preceding sections, some other notched beams tested by Kaplan (1961) and Körmeling & Reinhardt (1983) have been analysed. The optimum G_f values are summarized in Table 4.1, along with the specified concrete qualities. In this table the specimens have been so arranged that the material depth in front of the notch increases.

Firstly, it is notable that the optimum G_f-values for the various beams differ significantly although the specified concrete qualities do not differ appreciably. If G_f is indeed a material property, it seems to be an extremely sensitive one.

Table 4.1. Overview of data which suggest the fracture energy G_f to be a size-dependent property

experiment	max. agg. size mm	age days	w/c ratio	E N/mm^2	f_{ct} N/mm^2	optimum G_f bilinear softening N/m	optimum G_f linear softening N/m
NB Kaplan							
406 × 76 × 102 mm	12	28	0.5	29000	2.3	55	35
508 × 152 × 152 mm	12	28	0.5	29000	2.3	80	50
NB Körm./Reinh.							
450 × 100 × 100 mm	8	28	0.5	20000	2.4	113	70
NB Petersson							
2000 × 200 × 50 mm	12	28	0.5	30000	3.33	124	75
DCB Sok et al.							
2500 × 1100 × 300 mm	12	28	0.48	40000	4	350	250

NB = Notched Beam
DCB = Double Cantilever Beam

More serious however, is the fact that the table suggests G_f that increases with increasing specimen size. The discrepancies can partly be attributed to differences between loading equipment, testing conditions, loading speed, curing conditions and the slight variation in concrete qualities. However, most of these arguments do not hold when large and small beams of the same experimental program are compared with one another. Then, the analyses performed on the Kaplan experiments strongly suggest that G_f is size-dependent.

Possibly, the size-dependence of G_f has to do with the fact that fracture zones within small specimens are not allowed to develop fully, as explained in the preceding section. The likelihood that large specimens contain several fracture zones that remain undetected is an additional factor.

In future the size-dependence needs to be clarified, especially because we want to extrapolate the behaviour of small laboratory specimens to large structures like dams and piers. At present a great deal of experimental activity can already be reported in this field (see for instance Hillerborg, 1983, Cedolin, Dei Poli & Iori, 1983, Shah, 1984).

5 Mixed-mode fracture in unreinforced concrete

The preceding mode I examples were exceptional in that the crack path was purely straigth and directed parallel to the lines of the mesh. In structural practice cracks are seldom straight. Neither will they open purely in mode I, but their opening path will rather be a mix between mode I (crack opening displacements) and mode II (crack sliding displacements). In this chapter an intriguing example of mixed-mode fracture in unreinforced concrete is discussed.

5.1 *Finite element idealization for notched shear beam*

From among the scarce experiments on mixed-mode concrete fracture a notched shear beam, tested by Arrea & Ingraffea (1982), was selected for analysis. The supports and the loading conditions are non-symmetric with respect to the notch, as appears from Fig. 5.1 which shows the finite element idealization. Four-point reduced integrated quadratic elements were used. Note that the load was applied via a steel beam which

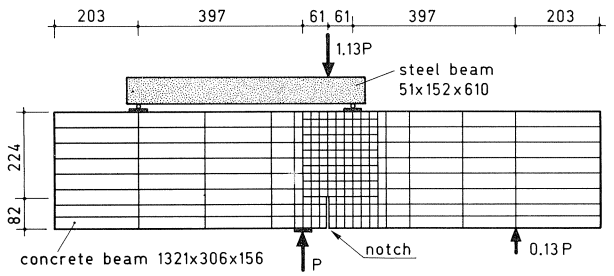

Fig. 5.1. Finite element idealization for notched unreinforced beam in mixed-mode fracture (dimensions in mm).

distributed it to the concrete beam. This steel beam was included in the mesh. Further, the bearing platens between the roller supports and the beam were so modelled as to assure proper load transfer into the specimen. The overlapping nodes from the bearing platens and concrete beam respectively were tied to each other in the vertical direction.

5.2 *Load-displacement response*

Fig. 5.2 presents the nonlinear response of the beam in terms of load-CMSD curves. The CMSD is the Crack Mouth Sliding Displacement, which is indicated. Although the maximum load is captured quite well, the numerical analysis predicts a post-peak response that is far too ductile compared with the experiment. Several reasons can be suggested for this discrepancy.

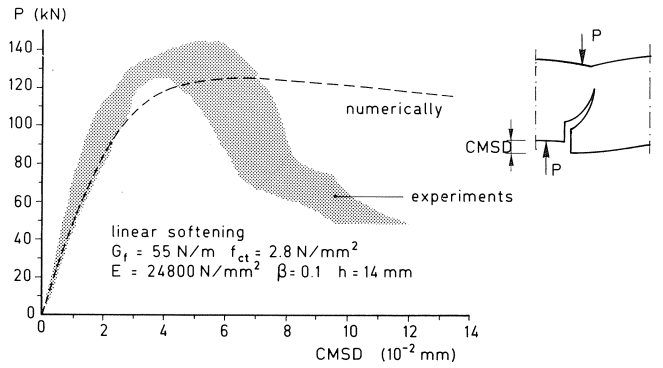

Fig. 5.2. Load vs. CMSD response for mixed-mode fracture problem (CMSD = Crack Mouth Sliding Displacement).

Firstly, the test was performed CMSD-controlled (the CMSD was the feedback for the hydraulic actuator on top of the steel beam), whereas the computation was carried out under control of the displacement at the loading point on top of the steel beam. Secondly, during the experiment cyclic loading was applied and holding stages were introduced so that the load "had the time" to decrease while the CMSD was kept constant. Such cyclic loading and time effects were not taken into account in the analysis. The third and major reason is that the numerical analysis was incapable of producing a fully converged solution in the post-peak regime. On the contrary, numerical instability occurred, which can be explained with reference to the predicted crack pattern, as will be done in the next section.

5.3 *Crack path*

The crack patterns are presented in Fig. 5.3, together with the corresponding plots of the deformations (of the mesh only the critical failure zone around the notch is shown). At maximum load only a limited number of Gauss-points appear to be cracked but im-

mediately after the peak unstable progressive cracking occurs and fracture is rapidly completed.

At first sight, the final crack pattern seems to be diffuse as the crack are spread over a wide band of approximately three elements. This would contrast with the experiment, where sharp discrete cracks have been observed. However, in the crack patterns a distinction has been made with regard to the actual size of the crack strain. Cracks with $\varepsilon_{nn}^{cr} > c\varepsilon_u$ are accentuated by means of thick lines, whereas the others are marked by normal lines (with this graphical facility, c is a factor that can be specified by the user; in Fig. 5.3, c was taken as 0.3).

With such distinction the picture changes drastically. Only a limited number of cracks appears to open widely, whereas the majority is arrested or even closed, in accordance with Fig. 2.2a. Omitting the arrested cracks (as in Fig. 5.5) is even more instructive. The diagrams reveal that cracking in fact localizes within a very narrow band of

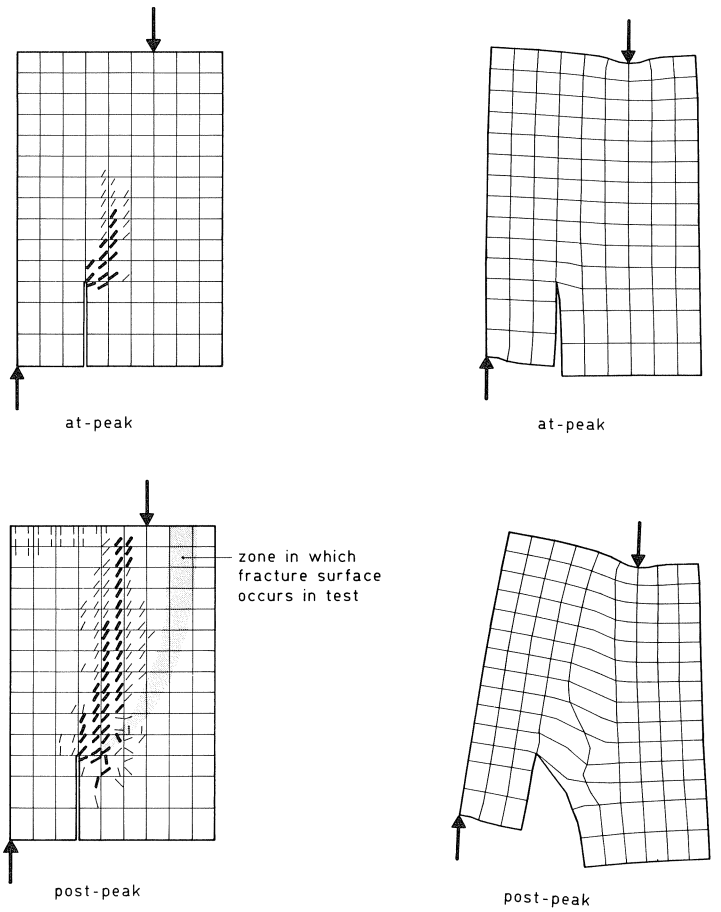

Fig. 5.3. Mixed-mode fracture problem. Crack pattern and deformations (amplification factor 200) at-peak and post-peak. Heavy dotted cracks are active cracks. Most of the light dotted cracks have been arrested or closed.

single integration-point width, which is emphasized by the inclusion of the plots of the deformations.

This possibility of predicting discrete cracks with a smeared approach is one of the most important conclusions to emerge from this study. This was already apparent for the unreinforced mode I examples and will later be demonstrated for reinforced concrete too. It is considered that the basic requirements for achieving such a high degree of strain localization are the implementation of the softening model, and in particular, of crack closing.

It must, however, immediately be added that problems are encountered too. One of them is that strain-localizations may introduce numerical instability. When a large number of cracks is initiated a serious problem is posed: which of these cracks open and which close or, in other words, where do the strains localize and where do they not? Suppose that two adjacent cracks are initiated simultaneously; then it is quite arbitrary whether crack 1 survives while crack 2 closes, or whether crack 2 survives while crack 1 closes. In any case, they cannot both open. Clearly, the equilibrium state is no longer unique but several alternative equilibrium states are possible. This phenomenon was investigated in detail by Crisfield (1982). He found that the presence of alternative equilibrium states may result in a badly conditioned system of equations. This is probably the prime reason why the post-peak behaviour of the present beam is highly unstable.

To overcome such problems with alternative equilibrium states a bifurcation analysis is required. Further, more sophisticated solution procedures than the Modified-Newton scheme applied at present are likely to improve post-peak convergence characteristics (e.g. Crisfield, 1983).

Another way to avoid problems is to reduce the number of alternative equilibrium states, or even to prevent them altogether. This can probably be achieved by taking into account the statistical scatter in strength properties. Then only the points with the lowest tensile strength will crack and soften, so that all deformation will localize at these weakest spots.

In addition to the problem with alternative equilibrium states there remains the constitutive problem of properly filling the crack interface matrix, eq. (2.7). The crack shear modulus G_c, which is related to the shear retention factor β according to eq. (3.11), was varied but did not affect the results positively. Neither did a change in G_f, which is linked with the softening modulus D_c^o. Probably, for this category of problems where shear as well as tensile stresses are transferred across the cracks, the assumption of zero off-diagonal terms in (2.7) is too simple. Instead, inserting some non-zero terms might be better. Physical justification of the magnitude of such terms will however be difficult as experimental results on coupled crack tension and crack shear are not, or only scarcely, available.

A final remark concerns the limitations that were encountered in predicting the curvilinear fracture surface. Fig. 5.3 shows that the predicted crack runs steeply and ends to the left of the load, whereas the experimental fracture surface was reported to take a large swing to the right and to meet the top of the beam to the right side of the load. Such steep crack paths were also found by other researchers using the smeared

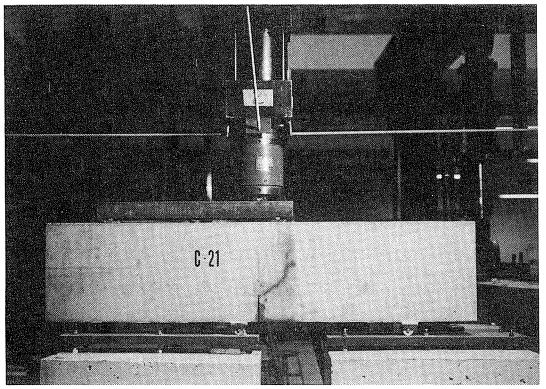

(a) Visualization of the crack which becomes the final fracture surface.
Obtained with water impregnation

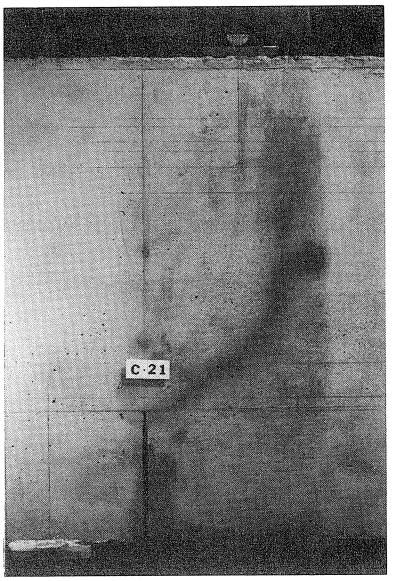

(b)
Close-up of (a)

(c)
Fracture surface

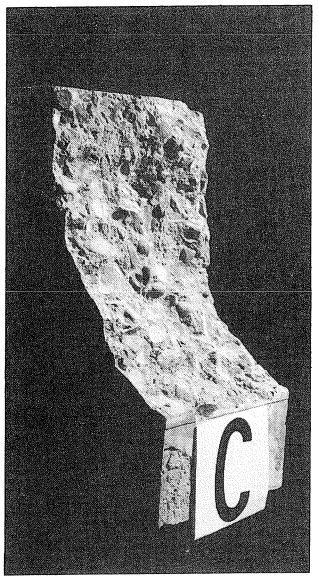

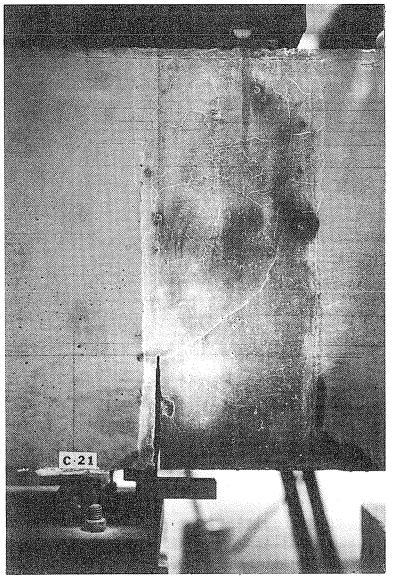

(d)
Visualization of at least two crack nucleation corridors.
Obtained with fluorescent particle penetrant

Fig. 5.4. Experimental results mixed-mode problem (Ingraffea, 1984).

concept (e.g. Glemberg, 1984), but not by discrete crack modellers (e.g. Arrea & Ingraffea, 1981, Wium, Buyukozturk & Li, 1984).

It should be emphasized that the experimental observation of only one final fracture surface (Figs. 5.4a to 5.4c) does not imply that there has also been only one individual crack. This was initially suggested by Arrea & Ingraffea (1982), but in a recent reinter-

pretation of the tests Ingraffea (1984) states that several individual crack nucleation corridors had been present before the specimen was completely fractured. The photograph in Fig. 5.4d shows this situation. We will return to this aspect in the next section.

5.4 *(In-)objectivity with respect to the chosen mesh*

The crack pattern in Fig. 5.3 suggests that the predicted crack favours a straight path parallel to the mesh lines before jumping into adjacent element rows. This prompted us to examine whether or not the choice for the mesh lines affects the final results.

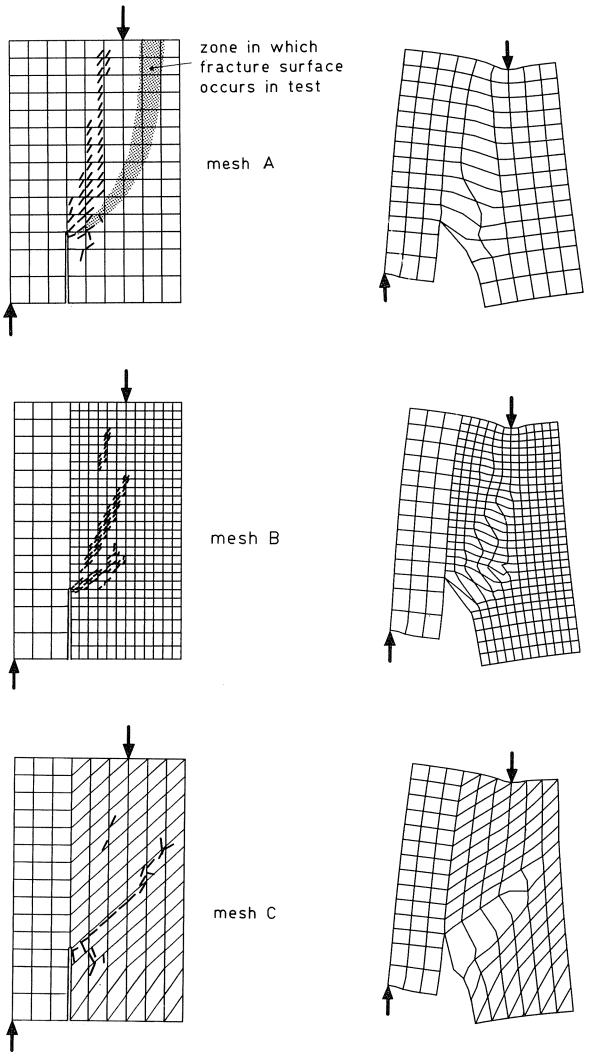

Fig. 5.5. Effect of mesh choice on finite element results for mixed-mode fracture problem. Strain localization occurs but the results are not objective.

In addition to the original mesh, which will be referred to as mesh A, two alternative meshes were considered:

- a refined mesh, shown as mesh detail B in Fig. 5.5 (for this mesh the orientation of the mesh lines was kept the same as for mesh A);
- an "inclined" mesh, shown as mesh detail C in Fig. 5.5 (for this mesh the orientation of the mesh lines was changed; the mesh was not refined with respect to mesh A).

Outside the depicted detail the mesh was kept the same as for mesh A. The results for the various meshes are compared to each other in Figs. 5.5 and 5.6.

Initially the crack through the refined mesh B follows the curvilinear trajectory. After a while, however, it is arrested and a second crack and later also a third crack develops within the area above the first trajectory. Agreement between this result and the photograph in Fig. 5.4d is good, so that the use of very fine meshes seems promising. Experimentally, only the first crack became the final fracture surface, which indicates that the other cracks in Fig. 5.4d must have closed. This situation occurred finally, i.e. far beyond the peak when the load had dropped to zero. Because of instabilities, however, it is not possible completely to keep track of this complex post-peak behaviour numerically. This explains why a final fracture surface has not been found for the fine mesh computation.

When comparing the results for mesh A and mesh B it can be said that in both cases crack formation localizes within the same region, to the left of the load. The conclusion is that the solution is fairly objective with respect to mesh refinements, which is accentuated by the close agreement between load-CMSD curves for mesh A and mesh B.

On the other hand, no objectivity is found with respect to the orientation of mesh lines. The load-CMSD curve for the inclined mesh C shows a departure from the curves corresponding to mesh A and B. Moreover, the predicted crack for mesh C propagates in a different direction, parallel to the inclined mesh lines. The crack indeed prefers to follow a straight path parallel to the element boundaries, just as for mesh A.

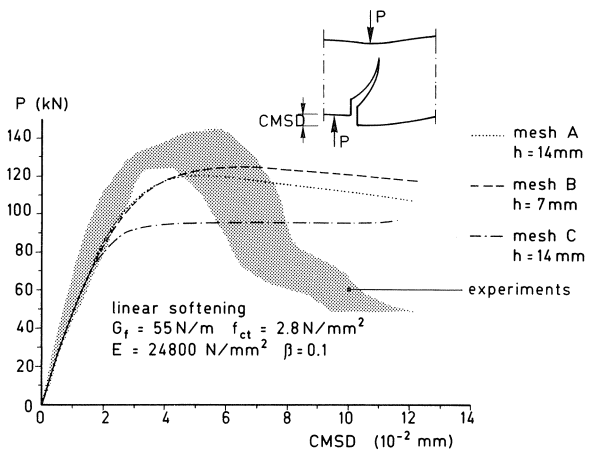

Fig. 5.6. Effect of mesh choice on load-CMSD response for mixed-mode fracture problem.

Such inobjectiveness is probably bound up with the fact that the Gauss-points are not equidistant, which is especially true if non-square elements are used. But even if square elements are taken, the diagonal distance between Gauss-points is $\sqrt{2}$ times as large as the straight distance between Gauss-points. This introduces a certain bias and is the prime reason why straight crack paths are favoured before diagonal crack jumps into adjacent rows of sampling points.

For mode I fracture analysis in combination with lower-order elements, objectivity for zig-zag crack band paths has to a certain extent been established (Bažant & Cedolin, 1983). In future it needs also to be achieved for mixed-mode cracks and other types of elements. Structural analysts choose their mesh subjectively, but in any case the solution ought to be objective.

6 Mixed-mode fracture in reinforced concrete

6.1 *Introductory remarks*

The preceding examples focussed on notched laboratory specimens exhibiting only one individual macro-crack. In most practical situations not just one but several macro-cracks will be induced, but even then one of the induced cracks may dominate the response while most of the others will be arrested. Such a situation is typical of shear-critical reinforced concrete beams, where the existence of vertical flexural cracks is overshadowed by a diagonal shear crack that suddenly occurs and dominates the failure behaviour.

Here, a couple of such beams will be discussed, which were selected from an experimental program carried out by Gijsbers & Smit (1977), also partially reported by Van den Beukel et al. (1981). The program was original in the sense that the beams were subjected to a uniformly distributed load, while the majority of tests reported in the literature has concentrated on three- or four-point loading systems. The distributed load implied that experiment as well as analysis had to be performed under load control rather than displacement control, which complicates establishing a genuine limit load.

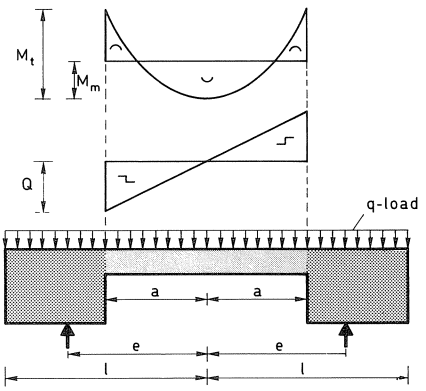

Fig. 6.1. Loading configuration for experiments on reinforced beams (Gijsbers & Smit, 1977).

As shown in Fig. 6.1, the actual beam was relatively small compared with the large supporting end-blocks that had been added in order to introduce the desired moment/shear ratios. By varying the sizes a, e and l this moment/shear ratio as well as the slenderness of the beam could be varied. In this way a wide range of shear failure mechanisms has been investigated, such as diagonal tension failure and shear-compression failure, which will both be considered here, in Sections 6.2 and 6.6 respectively.

The beams contained tensile as well as compressive reinforcement, but no stirrups. As has become customary (ASCE, 1982), reinforcement was modelled by means of bar elements that were embedded within the concrete elements. This simple representation implies overall perfect bond.

6.2 *Reinforced beam failing in diagonal tension*

For the first beam the bending moment at midspan amounts to three times the bending moment at the clamped end, resulting in a diagonal tension failure mode. The diagonal tension crack can be seen in Fig. 6.2, which shows the beam at experimental failure.

The data and finite element mesh used for this beam are shown in Fig. 6.3.

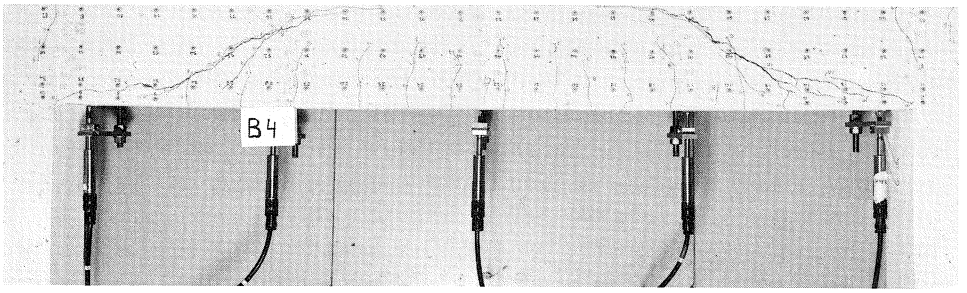

Fig. 6.2. Reinforced beam which failed in diagonal tension (Gijsbers & Smit, 1977).

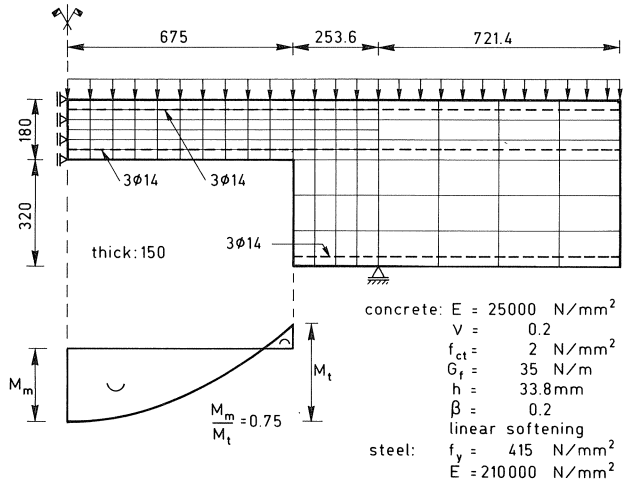

Fig. 6.3. Finite element idealization for reinforced beam which failed in diagonal tension (dimensions in mm).

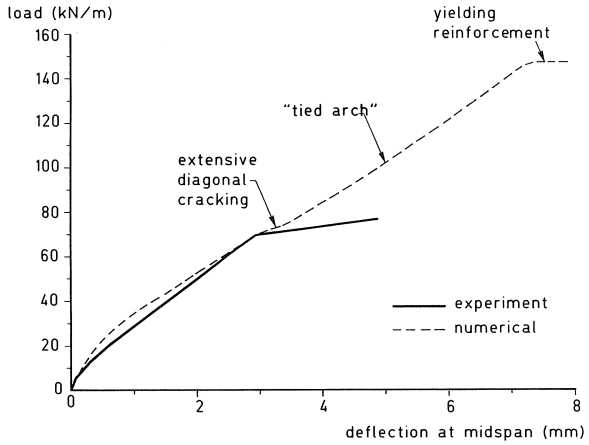

Fig. 6.4. Load-deflection response for reinforced beam which failed in diagonal tension.

The calculated load-deflection curves are compared to the experimental ones in Fig. 6.4. Characteristic of the experiment was the abrupt loss of stiffness in the final stage, which was due to the sudden development of the diagonal tension crack. At first sight, the numerical analysis appears to be incapable of reproducing this complex type of shear failure, as the load could be incremented until the reinforcement started yielding. However, closer examination of the numerical curve reveals a small but noteworthy irregularity, namely a decrease of stiffness at a loading level of about 73 kN/m.

It is very instructive to plot the crack patterns just before this irregularity ($q = 68$ kN/m) and just beyond it ($q = 75$ kN/m). This is done in Fig. 6.5. Note that these two loading levels roughly refer to impending experimental failure and experimental failure respectively. The diagram surprisingly reveals that it is not only the experiment but also the numerical analysis that leads to a dominant crack, developing solely within such a limited loading interval. Although the type of failure mechanism is thus reproduced quite well, it is rather disappointing that the numerical analysis does not indicate a clear corresponding limit load. The load-displacement response does not exhibit a peak or a horizontal plateau, but only shows the temporarily decrease in stiffness. Moreover, the applied Modified Newton-Raphson scheme was unable to produce a truly converged solution during the critical loading stage.

To achieve a genuine limit load and better convergence characteristics one should resort to more sophisticated solution procedures and apply arc-length control rather than load control (e.g. Crisfield, 1983). But even then one is left with the problem of alternative equilibrium states, as mentioned before, and with some inadequacies in constitutive modelling. In particular, there is the absence of a dowel action model and a bond-slip model, which both become important at impending failure.

Beyond the critical load interval the numerical analysis was able to find a new and stable equilibrium configuration associated with the transition from the beam to a "tied arch". Parallel to the diagonal cracks a concrete compressive arch was initiated which

was tied by the reinforcement. Very similar results were found by Dodds et al. (1982, 1984). Whether the tied arch must be regarded as an artificial numerical effect or as a realistic one is difficult to say, because during the experiment no attempt had been made to increase the load after the diagonal crack occurred. In fact, the experimental failure load is not genuine either, as failure occurred in a somewhat explosive manner, so that neither the load nor the displacements were properly controlled during the final stage.

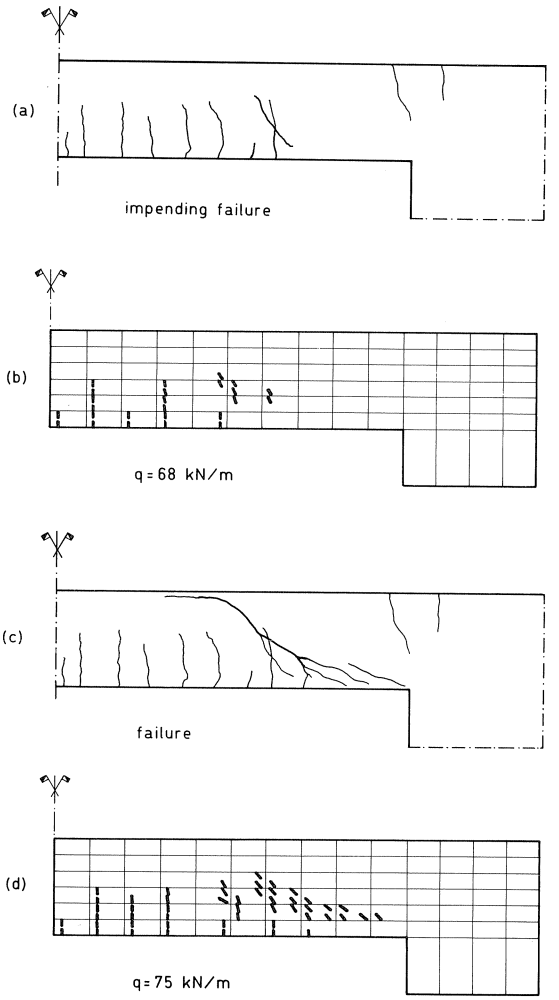

Fig. 6.5. Crack development in reinforced beam. Suddenly a diagonal tension crack occurred. Only full macro-cracks are shown.
(a) experimental, impending failure
(b) numerical, $q = 68$ kN/m
(c) experimental, failure (see also Fig. 6.2)
(d) numerical, $q = 75$ kN/m

6.3 *Detecting active cracks and arrested cracks*

It should be said that the numerical crack patterns depicted in Fig. 6.5 only display full cracks, i.e. cracks for which the normal crack strain is beyond the ultimate strain ε_u of the softening branch (compare Fig. 3.2). Partial cracks as well as closing cracks have been ignored in Fig. 6.5.

Whether this is misleading or not can be inferred from Fig. 6.6, which shows cracks with normal crack strains greater than $0.0\,\varepsilon_u$ (that is: all cracks), $0.2\,\varepsilon_u$, and $1.0\,\varepsilon_u$ (that is: only full cracks) respectively. The three plots refer to the same load level of $q = 75$ kN/m.

The difference between the plots reveals that, although the load is already beyond experimental failure, still a considerable number of Gauss-points exhibit cracks with only very small crack strains. Once formed, these cracks never fully developed but were arrested or were even closing and must therefore be regarded as "pseudo-cracks". Especially during the critical load interval (68–75 kN/m) the finite element outputs revealed that the diagonal cracks were very active while most of the existing vertical cracks were arrested and/or closing.

Just as with the mixed-mode problem in plain (unreinforced) concrete, we conclude that the implementation of a crack closing model is extremely important to achieve

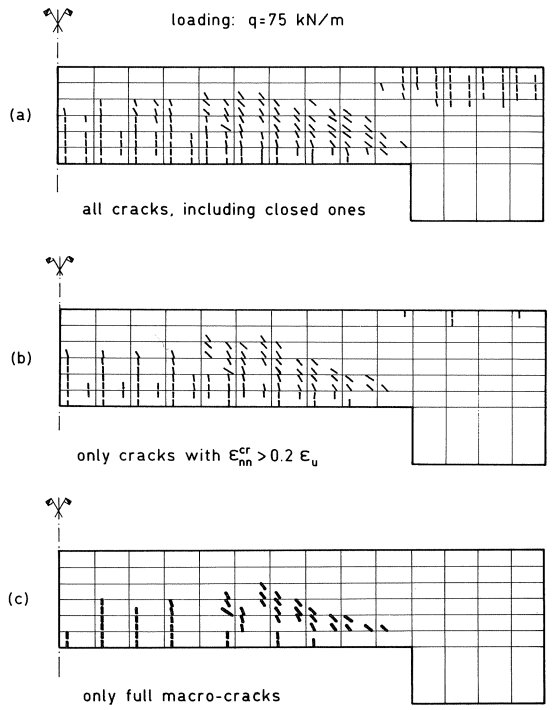

Fig. 6.6. Analysis of numerical crack pattern for reinforced beam. Displaying all cracks can be misleading. Displaying only full macro-cracks correctly reveals fracture localization.

strain localization. Currently a secant unloading branch is being used (Fig. 2.2) but a plastic-fracturing type of unloading branch could yield better results, as it is in closer agreement with experimental findings of, for instance, Reinhardt (1984). Further, unloading should be related to the crack shear relation too.

In the past smeared crack computations were sometimes judged on the basis of crack patterns like the one in Fig. 6.6a, where all cracks are plotted. Such interpretations may be grossly misleading. They suggest distributed failure and conceal the real fracture mechanism, which is highly local. To get a fair picture one should trace the active cracks and distinguish them from arrested ones. More illustrative examples are given by Rots (1983b), Van Foeken (1983) and De Borst & Nauta (1984).

6.4 *Effect of shear-retention factor*

In the past the shear retention factor β, alternatively to be expressed as a crack shear modulus G_c (eq. 3.10 and 3.11), has been the subject of much controversy, see for instance Schnobrich (1972), Cedolin & Dei Poli (1977, 1983) Ottosen (1982), ASCE (1982), Kolmar & Mehlhorn (1984), Crisfield (1984). Shear-critical problems are likely to depend on the particular choice for this factor, so that a parameter study is interesting.

In addition to the computation with $\beta = 0.2$ ($G_c = 0.25G$) as described above, two other computations were carried out, one for a very high value $\beta = 0.99$ ($G_c = 99G$), representing fully interlocked crack surfaces, and the other for a very low value $\beta = 0.01$ ($G_c \approx 0.01G$), simulating smooth and almost frictionless crack surfaces.

Fig. 6.7 reflects the effect on the load-displacement response, Fig. 6.8 compares the final crack patterns and Fig. 6.9 compares the incremental deformations during one of the critical load steps in which extensive cracking occurred.

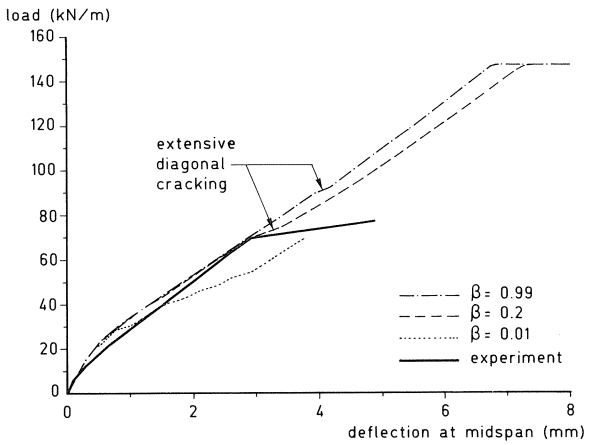

Fig. 6.7. Effect of shear retention factor β on load-deflection response for reinforced beam. The corresponding crack patterns and deformations are shown in Figs. 6.8 and 6.9.

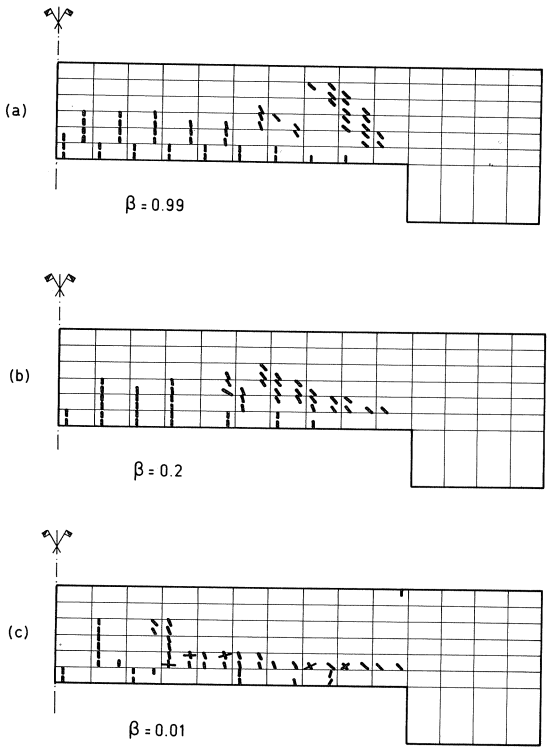

Fig. 6.8. Effect of shear retention factor β on crack pattern of reinforced beam.

The influence of β is found to be significant. The high value leads to the most distinct shear crack. For this computation all the deformation during the critical load steps appears to localize within a narrow band of elements (Figs. 6.8a and 6.9a).

For the intermediate value of β the localization of deformation is less pronounced, but still a final crack is visible, the location and inclination angle of which are in close agreement with the experiment (Figs. 6.8b and 6.9b).

For the very low β no diagonal cracking occurred at all. Instead, premature sliding occurred along the vertical cracks and a kind of horizontal shear plane was found just above the reinforcing layer (Figs. 6.8c and 6.9c). In addition convergence characteristics became poorer, which can be deduced from the load-displacement curve in Fig. 6.7, exhibiting "irregularities" all along the curve. Finally, numerical divergence occurred.

Similar arguments hold true for a variation in the softening modulus D_c. Very high values of D_c (i.e. steep softening paths) introduce numerical instabilities resulting in oscillating load-displacement curves and distorted crack patterns, whereas low values (i.e. shallow softening paths) yield good convergence characteristics and smooth load-deflection response as well as regular crack patterns. Details about the effect of D_c and some more parameters are given by Rots (1983b).

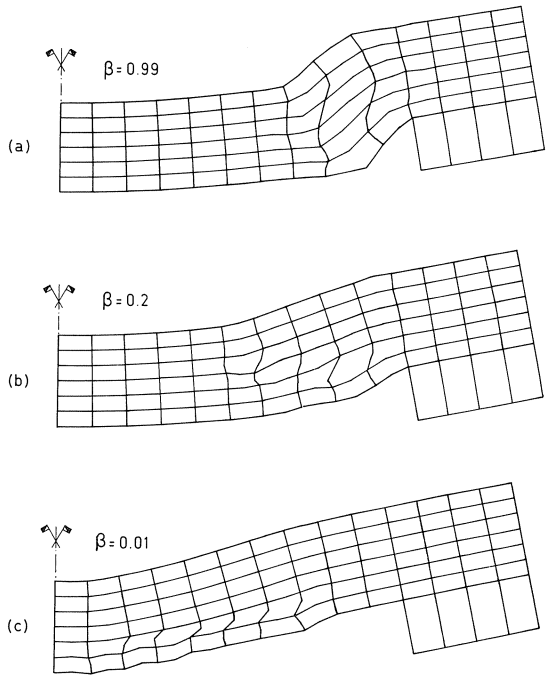

Fig. 6.9. Effect of shear retention factor β on incremental displacements during extensive diagonal cracking in reinforced beam.

6.5 *Need for continuing research*

The parameter studies in the preceding section indicate that additional basic research is required to establish more accurate expressions not only for G_c and D_c but also for the off-diagonal terms in the crack interface matrix (2.7). In any case, a constant value for G_c is unrealistic as it permits the crack shear stress to increase indefinitely. Partial improvements are achieved by employing a crack shear modulus which decreases with increasing normal crack strain (e.g. Cedolin & Dei Poli, 1977, Rots, Kusters & Nauta, 1984). In that case the crack shear stress does not increase indefinitely but reaches a certain plateau. The authors believe that further improvements can be achieved by adding shear softening and introducing mode II fracture energy.

Another aspect closely related to crack shear and to be clarified in future is the question of multiple cracks at the same sampling point, which may occur either if both principal stresses are tensile or if the principal stresses rotate significantly after the first crack was initiated. It is felt that the occurrence of multiple cracks heavily depends on the value adopted for β. For the present beam multiple cracks at the same sampling point occurred only for the very low value of β, as seen in Fig. 6.8c.

For all mixed-mode example problems reported here the eight-noded finite elements were integrated by means of the four-point reduced integration scheme, in order to save

computational effort. Recently, however, it has been suggested that reduced integration can introduce zero-energy modes and spurious cracking (Dodds, Darwin, Smith & Leibengood, 1982, Bergan, 1984). In the present investigations no indications of this were found, except in the computation for the very low shear retention factor. This aspect calls for further examination. Application of fully integrated eight-noded elements or, even better, fully integrated six-noded triangular elements is expected to be more reliable (Bergan, 1984).

Finally, the reader's attention is called to the "checkerboard" crack pattern in the neighbourhood of the tensile reinforcement, as appears from Figs. 6.8a and 6.8c. By coincidence, no checkerboard disturbance was found for the intermediate value of β; in that case the cracks crossed the reinforcement in a regular way, without jumps, Fig. 6.8b. Most probably, the existence of checkerboard patterns is related to the assumption of overall perfect bond between concrete and reinforcement, which tends to diffuse the crack pattern in the immediate surrounding of the reinforcing layer, as appears from Fig. 6.6. Consequently, almost every Gauss-point near the reinforcement cracks, so that the problem of the alternative equilibrium states, mentioned in Section 5.3, is very real there. A checkerboard pattern may be found, but alternatively a regular pattern may be found, depending on the precise choise of increment size, parameters, etc.

Anyhow, the perfect bond assumption conflicts with the delicate fracture mechanics treatment of individual cracks. More detailed modelling of the concrete-steel interface behaviour is likely to improve results. Attempts in this direction have for instance been made by Grootenboer (1979), De Groot, Kusters & Monnier (1981), Glemberg (1984) and Ingraffea, Gerstle, Gergely & Saouma (1984).

6.6 *Reinforced beam failing in shear-compression*

For the second beam the bending moment at the clamped end amounts to three times the bending moment at midspan. This resulted in a shear-compression failure mode, illustrated in Fig. 6.10, which shows the beam at experimental failure. Several splitting cracks are visible.

The data and finite element mesh used for this beam are shown in Fig. 6.11. For this analysis the concrete compressive stresses became very large, so that not only tensile cracking but also nonlinear behaviour of concrete in compression played an important

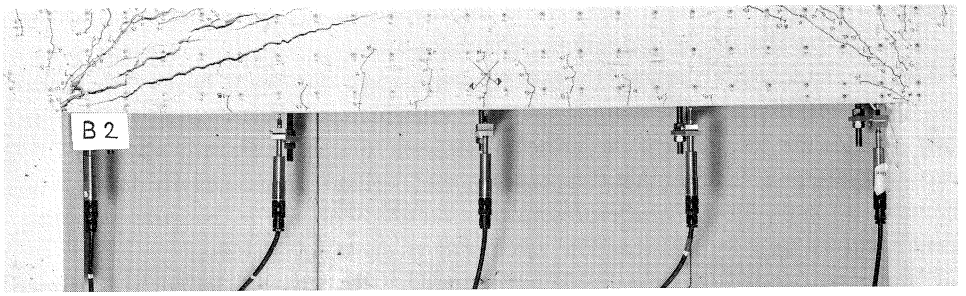

Fig. 6.10. Reinforced beam which failed in shear-compression (Gijsbers & Smit, 1977).

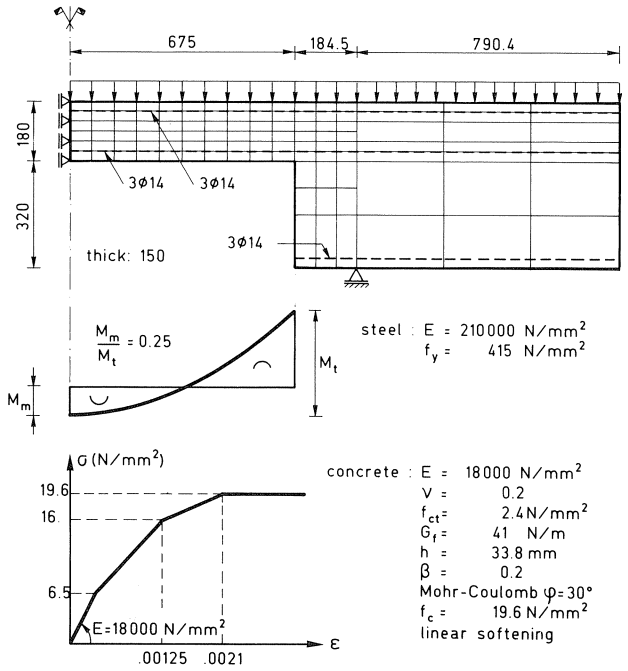

Fig. 6.11. Finite element idealization for reinforced beam which failed in shear-compression (dimensions in mm).

role. The constitutive model was therefore extended to include plasticity with isotropic cohesion hardening for concrete in compression. An associated flow rule and the Mohr-Coulomb yield criterion were adopted.

In Fig. 6.12 the load is plotted against the vertical displacement at midspan less the vertical displacement at the clamped end. Adding plasticity appeared to be essential to retrofit the ductile experimental response. In fact, a "plastic hinge" occurs in the com-

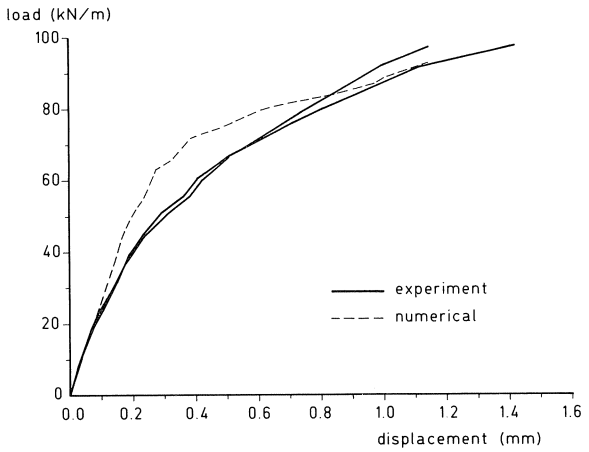

Fig. 6.12. Load-deflection response for reinforced beam failing in shear-compression.

pression zone near the clamped end. The computation was terminated when the maximum concrete compressive strain exceeded a value of 0.004, which corresponds to twice the strain at the peak of the uniaxial stress-strain diagram. Of course, this is a very rough failure criterion. Especially the addition of strain-softening in compression is likely to produce a better match with the experimental results (e.g. Ottosen, 1982). Such a softening model correctly will cause dominant cracks to penetrate into the compression zone, whereas the non-softening model overestimates the bending capacity of the beam, due to the indefinite ductility.

Crack development is represented in Fig. 6.13. The fracture mechanism differs fundamentally from that for the preceding beam in that diagonal splitting cracks were

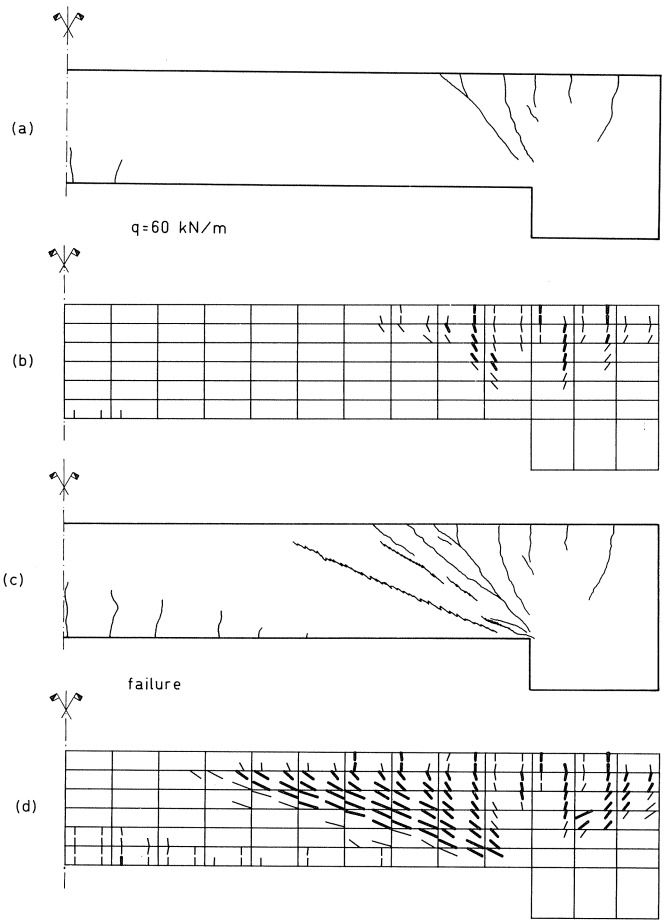

Fig. 6.13. Crack development in reinforced beam which failed in shear-compression due to diagonal splitting cracks. Full macro-cracks are emphasized by means of thick lines.
(a) experimental, $q = 60$ kN/m
(b) numerical, $q = 60$ kN/m
(c) experimental, failure (see also Fig. 6.10)
(d) numerical, failure

observed instead of a diagonal tension crack. Ultimately, the numerical cracks were spread over a fairly wide band, without pronounced localization. Between the cracks diagonal compression struts were active.

Such a splitting mode of failure makes severe demands on the constitutive model, as it covers a combination of tensile cracking with significant lateral compression. Strictly speaking, the present tensile strain-softening formulation is valid only for pure tensile fracture modes of failure, but does not apply to situations with significant lateral compression, as has been pointed out by Hillerborg (1984). On the other hand, the plasticity formulation primarily applies to the compression-compression region within the principal stress space. For the compression-tension region within this space a smooth transition between these extreme models is still to be developed. Recently, similar conclusions were drawn by Bićanić et al. (1984) and Willam (1984).

7 Concluding remarks

A smeared crack formulation has been proposed which treats concrete constitutive behaviour separately from crack interface behaviour. In this study concrete was in most cases modelled as a linearly elastic material, whereas for the crack the effects of tensile strain-softening, crack shear and crack closing were taken into account.

The model has shown to be promising for mode I fracture analysis of unreinforced concrete. For a variety of example problems close agreement with experimental data has been found, not only pre-peak but also post-peak. It is, however, felt that the results are extremely sensitive to the input of the concrete softening properties, such as the fracture energy and the shape of the softening branch. In this field experimental work is required to establish these properties solidly and to investigate their possible size-dependence, as is suggested by the present computations. For the mode I problems it has been demonstrated that the use of fracture energy in addition to strength parameters yields objective results that are independent of the chosen element sizes.

The latter conclusion only holds partially for the prediction of curvilinear mixed-mode cracks in unreinforced concrete. Especially when the crack path does not coincide with the orientation of the mesh lines, the final result appears to be mesh-dependent. Employing very fine meshes appears most attractive. For all meshes a high degree of strain localization was found, which is in close agreement with the experimental observations. Of the predicted cracks only a limited number turned out to be active, while the majority was arrested or even closed. However, a serious problem which accompanies strain localization is the numerical instability which can be induced by it.

Numerical instabilities partially vanished when stabilizing reinforcement was added. Analyses of shear-critical reinforced beams revealed sudden, extensive diagonal cracking within only a very limited number of load steps. Again, local cracks were thus shown to be represented surprisingly well, despite the fact that a smeared strategy has been followed. It should be added that the prediction of such shear fracture mechanisms is not always accompanied by finding a genuine corresponding peak-load and/or stable post-peak response, which may be attributed to the absence of advanced solution proce-

dures, but also to the absence of detailed models concerning bond-slip and dowel action.

The computational result for shear-critical beams depends very largely on the crack shear representation adopted. High shear retention factors yielded clear shear cracks, whereas very low values did not yield them at all and emphasized numerical instability. Further research should be stimulated to assess the complete crack interface matrix in agreement with experimental findings from laboratory tests.

Finally, it has been indicated that splitting modes of failure introduce additional difficulties, as they cover a combination of tensile strain-softening with significant lateral compression. There is need for a smooth transition between plasticity based models for concrete in compression and the strain-softening model for concrete in tension.

The principal outcome of this study is that the smeared crack strategy constitutes a promising tool for predicting fracture localization in concrete structures. Here, the strategy has been applied to studying individual cracks as though "under a magnifying glass", but numerous other investigations have shown that the smeared method is also suited to represent overall behaviour governed by global systems of densely distributed macro-cracks.

8 Acknowledgements

Partial financial support from the Netherlands Committee for Research, Codes and Specifications for Concrete (CUR-VB) and from the Netherlands Technology Foundation (STW) is gratefully acknowledged.

The authors would like to thank Frits de Witte and other members of the Software Engineering Department at the Institute TNO for Building Materials and Building Structures (TNO-IBBC) for continuously supporting software developments within the DIANA package. Thanks are also due tot René De Borst for his share in developing the numerical formulation of the crack model applied.

The numerical computations for this study were performed on the VAX 11/780 computer system operated by the Software Engineering Department at TNO-IBBC.

9 Notation

D_c or D_c^o	tensile strain-softening modulus
D_c^c	secant stiffness used for closing cracks
E	Young's modulus
f_{ct}	uniaxial tensile strength of concrete
f_c	uniaxial compressive strength of concrete
f_i	tensile strength limit
f_s	yielding strength of steel
G	elastic shear modulus
G_c	crack shear modulus
g_f	area under strain-softening diagram

G_f	fracture energy
h	crack band width
β	shear retention factor
ε, γ	total strains
$\varepsilon^{co}, \gamma^{co}$	concrete strains
$\varepsilon_{xx}^{cr}, \varepsilon_{yy}^{cr}, \gamma_{xy}^{cr}$	global crack strains
$\varepsilon_{nn}^{cr}, \gamma_{nt}^{cr}$	local crack strains
ε_u	ultimate strain of the tensile strain-softening diagram
ν	Poisson's ratio
$\sigma_{xx}, \sigma_{yy}, \sigma_{xy}$	global stresses
σ_{nn}, σ_{nt}	crack interface stresses

10 References

ARREA, M & A. R. INGRAFFEA (1982), Mixed-mode crack propagation in mortar and concrete. Report No. 81-13, Department of Structural Engineering, Cornell University, Ithaca, New York.

ASCE (1982), State-of-the-art report on finite element analysis of reinforced concrete. Prepared by a Task Committee chaired by A. Nilson, American Society of Civil Engineers, New York.

BAŽANT, Z. P. & L. CEDOLIN (1979), Blunt crack band propagation in finite element analysis. Journal of the Engineering Mechanics Division, ASCE, Vol. 105, No. EM2, pp. 297–315.

BAŽANT, Z. P. & P. GAMBAROVA (1980), Rough cracks in reinforced concrete. Journal of the Structural Division, ASCE, Vol. 106, No. ST4, pp. 819–842.

BAŽANT, Z. P. & L. CEDOLIN (1983), Finite element modeling of crack band propagation. Journal of Structural Engineering, ASCE, Vol. 109, No. ST1, pp. 69–92.

BAŽANT, Z. P. & B. H. OH (1983), Crack band theory for fracture of concrete. Materials and Structures, RILEM, Vol. 16, No. 94, pp. 155–177.

BAŽANT, Z. P., T. B. BELYTSCHKO & T. P. CHANG (1984), Continuum theory for strain-softening. Journal of Engineering Mechanics, Vol. 110, No. 12.

BAŽANT, Z. P. (1984), Imbricate continuum and its variational derivation. Journal of Engineering Mechanics, Vol. 110, No. 12.

BERGAN, P. G. (1984), Some aspects of interpolation and integration in nonlinear finite element analysis of reinforced concrete structures. Computer-Aided Analysis and Design of Concrete Structures (eds. F. Damjanić et al.), Pineridge Press, Swansea, United Kingdom, pp. 301–316.

BEUKEL, A. VAN DEN, J. BLAAUWENDRAAD, P. J. G. MERKS & TH. MONNIER (1981), Shear failure of beams: experiments and analysis. IABSE Colloquium on Advanced Mechanics of Reinforced Concrete, Delft, pp. 509–520.

BIĆANIĆ, N., S. STURE, B. HURLBUT & S. DAY (1984), On the prediction of the peak and post-peak behavior of concrete structures. Computer-Aided Analysis and Design of Concrete Structures (eds. F. Damjanić et al.), Pineridge Press, Swansea, United Kingdom, pp. 245–259.

BLAAUWENDRAAD, J. & H. J. GROOTENBOER (1981), Essentials for discrete crack analysis. IABSE Colloquium on Advanced Mechanics of Reinforced Concrete, Delft, pp. 263–272.

BORST, R. DE, G. M. A. KUSTERS, P. NAUTA & F. C. DE WITTE (1983), DIANA – a comprehensive, but flexible finite element system. Finite Element Systems Handbook, Third Edition, Springer Verlag, Berlin, Germany.

BORST, R. DE, G. M. A. KUSTERS, P. NAUTA & F. C. DE WITTE (1984), DIANA, a threedimensional, nonlinear finite element package on a micro-computer. Engineering Software for Microcomputers (eds. B. A. Schrefler et al.), Pineridge Press, Swansea, United Kingdom, pp. 435.

BORST, R. DE & P. NAUTA (1984), Smeared crack analysis of reinforced concrete beams and slabs failing in shear. Computer-Aided Analysis and Design of Concrete Structures (eds. F. Damjanić et al.), Pineridge Press, Swansea, United Kingdom, pp. 261–273.

CEDOLIN, L. & S. DEI POLI (1977), Finite element studies of shear critical reinforced concrete beams. Journal of the Engineering Mechanics Division, ASCE, Vol. 103, No. EM3, pp. 395–410.

CEDOLIN, L. & S. DEI POLI (1983), Discussion of "2-D finite element analysis of massive R/C structures", by Ottosen. Journal of Structural Engineering, Vol. 109, No. 10, pp. 2479-2481.
CEDOLIN, L., S. DEI POLI & I. IORI (1983), Experimental determination of the fracture process zone in concrete. Cement and Concrete Research, Vol. 13, No. 4, pp. 557-567.
CRISFIELD, M. A. (1982), Local instabilities in non-linear analysis of reinforced concrete beams and slabs. Proceedings Institution of Civil Engineers, Part 2, No. 73, pp. 135-145.
CRISFIELD, M. A. (1983), An arc-length method including line searches and accelerations. International Journal for Numerical Methods in Engineering, Vol. 19, pp. 1269-1289.
CRISFIELD, M. A. (1984), Difficulties with current numerical models for reinforced-concrete and some tentative solutions. Computer-Aided Analysis and Design of Concrete Structures (eds. F. Damjanić et al.), Pineridge Press, Swansea, United Kingdom, pp. 331-357.
DODDS, R. H., D. DARWIN, J. L. SMITH & L. D. LEIBENGOOD (1982), Grid size effects with smeared cracking in finite element analysis of reinforced concrete. SM Report No. 6, University of Kansas Center for Research, Lawrance, Kansas.
DODDS, R. H., D. DARWIN & L. D. LEIBENGOOD (1984), Stress controlled smeared cracking in r/c beams. Journal of Structural Engineering, Vol. 110, No. 9, pp. 1959-1976.
EVANS, R. H. & M. S. MARATHE (1968), Microcracking and stress-strain curves for concrete in tension. Materiaux et Constructions, Vol. 1, No. 1, pp. 61-64.
FOEKEN, R. J. VAN (1983), Prediction of crack patterns and load-deflection curves of some reinforced concrete benchmark problems with DIANA. Report No. BI-83-40, Institute TNO for Building Materials and Building Structures, Rijswijk, The Netherlands.
GIJSBERS, F. B. J. & C. L. SMIT (1977), Resultaten van de eerste serie dwarskrachtproeven. Report No. BI-77-128, Institute TNO for Building Materials and Building Structures, Rijswijk.
GLEMBERG, R. (1984), Dynamic analysis of concrete structures. Publication 84:1, Department of Structural Mechanics, Chalmers University of Technology, Göteborg, Sweden.
GROOT, A. K. DE, G. M. A. KUSTERS & TH. MONNIER (1981), Numerical modelling of bond-slip behaviour. HERON Vol. 26, Special Publication on Concrete Mechanics No. 1B.
GROOTENBOER, H. J. (1979), Finite element analysis of two-dimensional reinforced concrete structures, taking account of nonlinear physical behaviour and the development of discrete cracks. Doctoral Thesis, Delft University of Technology, Delft, The Netherlands.
GROOTENBOER, H. J., S. F. C. H. LEYTEN & J. BLAAUWENDRAAD (1981), Numerical models for reinforced concrete structures in plane stress. HERON Vol. 26, Special Publication on Concrete Mechanics No. 1c.
HAND, R. H., D. A. PECKNOLD & W. C. SCHNOBRICH (1973), Nonlinear layered analysis of RC plates and shells. Journal of the Structural Division, ASCE, Vol. 99, No. ST7, pp. 1491-1505.
HEILMANN, H. G., H. H. HILSDORF & K. FINSTERWALDER (1969), Festigkeit und Verformung von Beton unter Zugspannungen. Deutscher Ausschuss fur Stahlbeton, Heft 203, W. Ernst & Sohn, West Berlin, Germany.
HILLERBORG, A., M. MODEER & P. E. PETERSSON (1976), Analysis of crack formation and crack growth in concrete by means of fracture mechanics and finite elements. Cement and Concrete Research, Vol. 6, No. 6, pp. 773-782.
HILLERBORG, A. (1983), Concrete fracture energy tests performed by 9 laboratories according to a draft RILEM recommendation. Report Nos. TVBM-3015 and TVBM-3017, Division of Building Materials, Lund Institute of Technology, Lund, Sweden.
HILLERBORG, A. (1984), Numerical methods to simulate softening and fracture of concrete. To be published in: Fracture Mechanics of Concrete (eds. G. C. Sih & A. Di Tomasso), Martinus Nijhoff Publishers, The Hague, The Netherlands.
INGRAFFEA, A. R. & V. SAOUMA (1984), Numerical modeling of discrete crack propagation in reinforced and plain concrete. To be published in: Fracture Mechanics of Concrete (eds. G. C. Sih & A. Di Tomasso), Martinus Nijhoff Publishers, The Hague, The Netherlands.
INGRAFFEA, A. R., W. H. GERSTLE, P. GERGELY & V. SAOUMA (1984), Fracture mechanics of bond in reinforced concrete. Journal of Structural Engineering, ASCE, Vol. 110, No. 4, pp. 871-890.
INGRAFFEA, A. R. (1984), Private communication.
KAPLAN, M. F. (1961), Crack propagation and the fracture of concrete. Journal of the American Concrete Institute, Vol. 58, No. 5, pp. 591-609.

KOLMAR, W. & G. MEHLHORN (1984), Comparison of shear stiffness formulations for cracked reinforced concrete elements. Computer-Aided Analysis and Design of Concrete Structures (eds. F. Damjanić et al.), Pineridge Press, Swansea, United Kingdom, pp. 133–147.

KÖRMELING, H. A. & H. W. REINHARDT (1983), Determination of the fracture energy of normal concrete and epoxy modified concrete. Report No. 5-83-18, Stevin Laboratory, Delft University of Technology, Delft, The Netherlands.

LEIBENGOOD, L. D., D. DARWIN & R. H. DODDS (1984), Finite element analysis of concrete fracture specimens. SM Report No. 11, University of Kansas Center for Research, Lawrence, Kansas.

LIN, C.-S. & A. C. SCORDELIS (1975), Nonlinear analysis of RC shells of general form. Journal of the Structural Division, ASCE, Vol. 101, No. ST3, pp. 523–538.

LITTON, R. W. (1976), A contribution to the analysis of concrete structures under cyclic loading. Dissertation, University of California, Berkeley.

NGO, D. & A. C. SCORDELIS (1967), Finite element analysis of reinforced concrete beams. Journal of the American Concrete Institute, Vol. 64, No. 3, pp. 152–163.

NILSSON, L. & M. OLDENBURG (1983), Nonlinear wave propagation in plastic fracturing materials – A constitutive modelling and finite element analysis. IUTAM Symposium Nonlinear Deformation Waves, (ed. U. Nigul and J. Engelbrecht), Springer Verlag, Berlin, Germany.

OTTOSEN, N. S. (1982), 2-D Finite element analysis of massive RC structures. Journal of the Structural Division, ASCE, Vol. 108, No. ST8, pp. 1874–1893.

PETERSSON, P. E. (1981), Crack growth and development of fracture zones in plain concrete and similar materials. Report No. TVBM-1006, Division of Building Materials, University of Lund, Sweden.

RASHID, Y. R. (1968), Analysis of prestressed concrete pressure vessels. Nuclear Engineering and Design, Vol. 7, No. 4, pp. 334–344.

REINDHARDT, H. W. (1984), Fracture mechanics of an elastic softening material like concrete. HERON, Vol. 29, No. 2.

ROTS, J. G. (1983a), Analysis of crack propagation and fracture of concrete with DIANA. Report No. BI-83-26, Institute TNO for Building Materials and Building Structures, Rijswijk, The Netherlands.

ROTS, J. G. (1983b), Prediction of dominant cracks using the smeared crack concept. Report No. BI-83-39, Institute TNO for Building Materials and Building Structures, Rijswijk, The Netherlands.

ROTS, J. G., G. M. A. KUSTERS & P. NAUTA (1984), Variabele reductiefactor voor de schuifweerstand van gescheurd beton. Report No. BI-84-33, Institute TNO for Building Materials and Building Structures, Rijswijk, The Netherlands.

ROTS, J. G., G. M. A. KUSTERS & J. BLAAUWENDRAAD (1984), The need for fracture mechanics options in finite element models for concrete structures. Computer-Aided Analysis and Design of Concrete Structures (eds. F. Damjanić et al.), Pineridge Press, Swansea, United Kingdom, pp. 19–32.

SCHNOBRICH, W. C. et al. (1972), Discussion of "Nonlinear stress analysis of reinforced concrete", by Valliapan & Doolan. Journal of the Structural Division, Vol. 98, pp. 2327–2328.

SHAH, S. P. (ed.) (1984), Preprints of the Proceedings NATO Advanced Workshop on "Application of fracture mechanics to cementitious materials". Northwestern University, Evanston, U.S.A.

SOK, C., J. BARON & D. FRANÇOIS (1979), Mécanique de la rupture appliquée au béton hydraulique. Cement and Concrete Research, Vol. 9. pp. 641–648.

SUIDAN, M. & W. C. SCHNOBRICH (1973), Finite element analysis of reinforced concrete. Journal of the Structural Division, ASCE, Vol. 99, No. ST10, pp. 2109–2122.

WALRAVEN, J. C. (1980), Aggregate interlock: a theoretical and experimental analysis. Dissertation, Delft University of Technology, Delft, The Netherlands.

WILLAM, K. J. (1984), Experimental and computational aspects of concrete fracture. Computer-Aided Analysis and Design of Concrete Structures (eds. F. Damjanić et al.), Pineridge Press, Swansea, United Kingdom, pp. 33–69.

WIUM, D. J. W., O. BUYUKOZTURK & V. C. LI (1984), Hybrid model for discrete cracks in concrete. Journal of Engineering Mechanics. ASCE, Vol. 110, No. 4, pp. 1211–1229.

APPENDIX I

Comparison with the crack band model proposed by Bažant & Oh

When certain conditions are satisfied it can be shown that the crack model, presented in Chapter 2, reduces to a direct formulated model which is not based upon a resolution of the total strain.

One such mode[1] is the mode I crack band model proposed by Bažant & Oh (1983), which in compliance formulation reads

$$\begin{bmatrix} \Delta\varepsilon_{nn} \\ \Delta\varepsilon_{tt} \end{bmatrix} = \begin{bmatrix} \frac{1}{E_t} & -\frac{\nu}{E} \\ -\frac{\nu}{E} & \frac{1}{E} \end{bmatrix} \begin{bmatrix} \Delta\sigma_{nn} \\ \Delta\sigma_{tt} \end{bmatrix} \tag{I.1}$$

in which n, t refer to the crack axes, E and ν are the elastic properties and E_t is the softening modulus indicated in Fig. I.1.

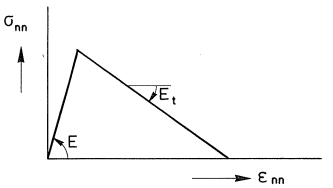

Fig. I.1. Tensile strain-softening modulus E_t for crack band model proposed by Bažant & Oh (1983).

Several researchers have extended this model to a mixed-mode model by adding a shear retention factor. Doing so, and inverting the compliance matrix, yields the following stress-strain relation (e.g. Rots, 1983a, 1983b)

$$\begin{bmatrix} \Delta\sigma_{nn} \\ \Delta\sigma_{tt} \\ \Delta\sigma_{nt} \end{bmatrix} = \begin{bmatrix} \frac{EE_t}{E-\nu^2E_t} & \frac{\nu EE_t}{E-\nu^2E_t} & 0 \\ \frac{\nu EE_t}{E-\nu^2E_t} & \frac{E^2}{E-\nu^2E_t} & 0 \\ 0 & 0 & \frac{\beta E}{2(1+\nu)} \end{bmatrix} \begin{bmatrix} \Delta\varepsilon_{nn} \\ \Delta\varepsilon_{tt} \\ \Delta\gamma_{nt} \end{bmatrix} \tag{I.2}$$

The model presented in Chapter 2 leads to (see eq. 2.12)

$$\Delta\boldsymbol{\sigma} = [\mathbf{D}^{co} - \mathbf{D}^{co}\mathbf{N}[\mathbf{D}^{cr} + \mathbf{N}^T\mathbf{D}^{co}\mathbf{N}]^{-1}\mathbf{N}^T\mathbf{D}^{co}]\,\Delta\boldsymbol{\varepsilon} \tag{I.3}$$

in which

$\Delta\boldsymbol{\varepsilon}$ = vector of global strain increments
$\Delta\boldsymbol{\sigma}$ = vector of global stress increments

$\mathbf{D}^{co}$ = incremental stress-strain matrix for concrete (eq. 2.8)
$\mathbf{D}^{cr}$ = crack interface matrix (eq. 2.7)
$\mathbf{N}$ = crack strain transformation matrix (eq. 2.2)

Now, suppose that

1. only one crack occurs at a sampling point and that the global x,y axes coincide with the crack axes n,t; then

$$\mathbf{N}=\begin{bmatrix} 1 & 0 \\ 0 & 0 \\ 0 & 1 \end{bmatrix} \tag{I.4}$$

2. concrete behaves linearly elastic, so that

$$\mathbf{D}^{co}=\frac{E}{1-\nu^2}\begin{bmatrix} 1 & \nu & 0 \\ \nu & 1 & 0 \\ 0 & 0 & \frac{1-\nu}{2} \end{bmatrix} \tag{I.5}$$

3. the crack interface matrix is of the form

$$\mathbf{D}^{cr}=\begin{bmatrix} D_c & 0 \\ 0 & G_c \end{bmatrix} \tag{I.6}$$

which alternatively can be expressed with the aid of eq. 3.9 and 3.11 as

$$\mathbf{D}^{cr}=\begin{bmatrix} \frac{EE_t}{E-E_t} & 0 \\ 0 & \frac{\beta}{1-\beta}G \end{bmatrix} \tag{I.7}$$

Substituting eq. I.4, I.5 and I.7 into I.3 yields, after extensive elaboration, a constitutive equation which is exactly similar to eq. I.2. Hence, both types of models are proved to be equivalent if the three above mentioned conditions are satisfied.

APPENDIX II

Crack band width

When estimating the crack band width and confining attention to rectangular quadratic elements, it is convenient to distinguish between three cases:

1. Mode I cracks for which the crack band path is parallel to the lines of the mesh and known in advance, as shown in Fig. II.1a.
   The symmetry of these problems implies that the final crack localizes within the width that belongs to the entire finite element. (The width is measured in the direc-

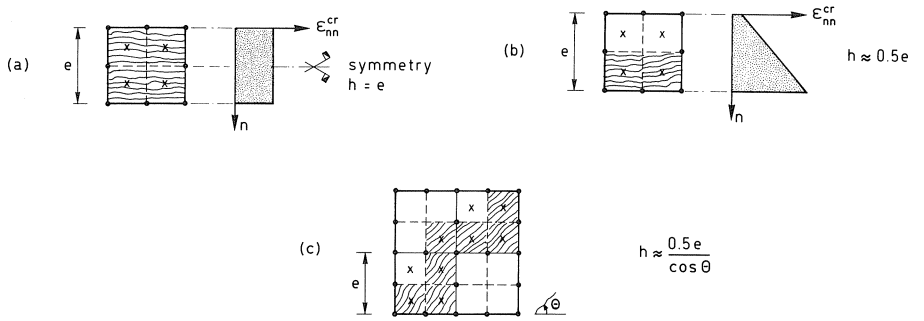

Fig. II.1. Estimates of the crack band width h in different circumstances.
(a) symmetric mode I problem
(b) non-symmetric problem but crack path parallel to mesh lines
(c) arbitrary crack path

tion normal to the crack.) Hence, the crack is smeared out over three Gauss points in the case of full integration, and over two Gauss points in the case of reduced integration.

Further, observe from Fig. II.1a that symmetry involves a constant strain distribution over the crack band, so that relation 3.5 ($G_f = hg_f$) holds exactly.

2. Cracks for which the crack band path is approximately parallel to the lines of the mesh and known in advance, as shown in Fig. II.1b.

   For such problems it is fair to assume that the crack tends to localize within one integration point. Consequently, when reduced four-point integration is used, the crack band width equals half the width that belongs to the finite element. This situation is typical of many structures in practice, such as reinforced beams. Here, one fortunately knows in advance that cracks will arise almost vertically, i.e. parallel to the lines of the mesh.

   In these cases the strain distribution over the crack band width will not be constant, but linear, as shown in Fig. II.1b. As the Gauss-point is located close to the center of the crack band, the strain at the Gauss-point is almost equal to the mean strain at the center of the crack band. Consequently, eq. 3.5 ($G_f = hg_f$) does not hold exactly, but can be applied as a fair approximation.

3. Cracks for which the crack band path does not follow the lines of the mesh and is not known in advance, as shown in Fig. II.1c.

   Such cracks zig-zag through the mesh. Confining attention to square elements, a reasonable approximation of the crack band width has been given by Bažant & Oh (1983). Their formula is added to Fig. II.1c. For the mixed-mode fracture problem described in Chapter 5, the angle θ was assumed to be 45°.

The formulae given in Fig. II.1 constitute only rough estimates of the crack band width. When accurate predictions of quantitative behaviour are desired, it is better to delay estimation of h till the crack is initiated and the crack angle has been registrated. Now, the estimates have been made in advance.